

Lifetime Measurement of the Metastable 2^3P_0 state in He-like Au⁷⁷⁺

S. Toleikis¹, B. Manil², E. Berdermann¹, H.F. Beyer¹, B. Birkett⁴, F. Bosch¹,
M. Czanta¹, R.W. Dunford⁶, P. Indelicato², C. Kozhuharov¹, D. Liesen¹, X. Ma¹,
R. Marrus⁴, P.H. Mokler¹, D. Schneider⁵, A. Simionovici³, Th. Stöhlker¹, Y. Zou⁷

¹GSI, Darmstadt, Germany, ²Université P. et M. Curie, Lab. Kastler Brossel, Paris, France,

³European Synchrotron Radiation Facility (ESRF), Grenoble, France, ⁴University of California, Berkeley, U.S.A.,

⁵Lawrence Livermore National Laboratory, Livermore, U.S.A., ⁶Argonne National Laboratory, Argonne, U.S.A.,

⁷Jiaotong University, Shanghai, China

The $2^3P_1 - 2^3P_0$ fine-structure splitting has been and still is a subject of experimental and theoretical interest in atomic physics. While in low-Z systems for neutral helium and Li^+ very accurate calculations have been carried out in the 70's, for helium-like high-Z ions new methods were needed to determine this fine structure splitting. Meanwhile, different theoretical approaches exist [1, 2, 3] and one aim of the experiment is to test which approach can give the correct values for the fine structure. For the high-Z region, only few measurements are available so far [4, 5]. Although this fine structure splitting is not directly measurable presently, it has been shown that this splitting can be determined indirectly by measuring the hyperfine-quenched lifetime of the 2^3P_0 state [6]. Due to the hyperfine interaction, the metastable 2^3P_0 state couples to the prompt 2^3P_1 state and the coupling strength depends on the $2^3P_1 - 2^3P_0$ fine-structure splitting. Thereby, the lifetime of the pure 2^3P_0 state is reduced and the fine-structure splitting can be determined.

The basic method to measure the lifetime of the hyperfine quenched 2^3P_0 state is beam foil spectroscopy. This rather simple method is illustrated in Figure 1, where the setup of the experiment performed at Cave A in August 2000 is shown. A hydrogen-like gold beam with an energy of 194.8 MeV/u ($\beta = 0.5621$) passes through a target foil (1.5 mg/cm² Ni) and hereby produces excited helium-like ions by electron capture. The radiation of the subsequent decay of the excited states is detected downstream of the foil by two Ge(i) detectors, located on opposite sides of the beam. The position of one detector is fixed while the other detector is moveable. By varying the distance between the target foil and the moveable detector and by measuring the ratio of counts of the $2^3P_0 - 1^1S_0$ -transition in the moveable detector relative to the fixed detector, a decay curve can be traced out. Measuring the ratio allows normalization to the ion population in the excited state of interest and has the additional advantage that most systematic errors are eliminated.

In contrast to the old experiment performed in 1994 [7], now for the first time, it was possible to measure the x-rays in coincidence with the down-charged helium-like ions, because recently a charge state spectrometer consisting of a quadropole doublet and a bending magnet has been installed in Cave A. An experiment to determine projectile ionization cross sections, performed one year ago, has served as a commissioning test and has shown the ability of the spectrometer to separate the different charge states [8]. In order to benefit from the charge state separation one also needs a position sensitive particle detector. Therefore a newly developed 32-fold strip diamond detector with a detection area of 60*40 mm² has been installed after the bending magnet. The advantages of this new type of particle detector are its time resolution below 50 ps and espe-

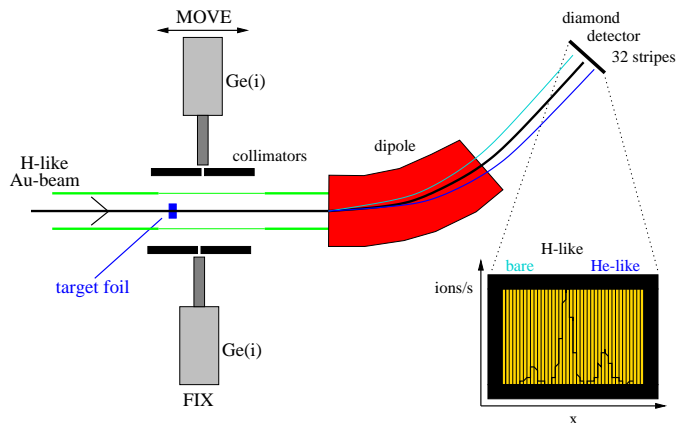


Figure 1: Experimental setup in Cave A.

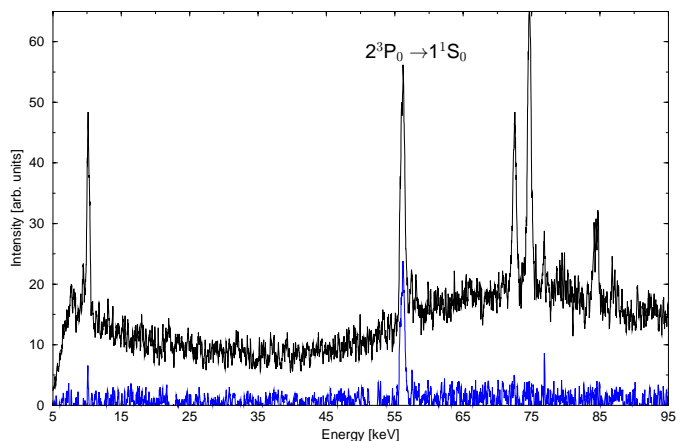


Figure 2: A raw and a coincidence spectrum obtained with the moveable Ge(i) detector.

cially its single-particle count-rate capability of up to 10⁸ ions/s [9].

Figure 2 now shows two sample energy spectra of the moveable x-ray detector. The upper spectrum shows a raw energy spectrum without coincidence condition while the lower one shows an energy spectrum obtained in coincidence with helium-like ions. The advantage of the coincidence technique is obvious.

The results of a preliminary analysis of the obtained data can be seen in Figure 3. Decay curves at two different positions of the fixed detector resulting in different normalisations have been traced out, covering almost three decay lengths. In addition, to have a comparison with the old experiment also a decay curve without coincidence requirement has been mea-

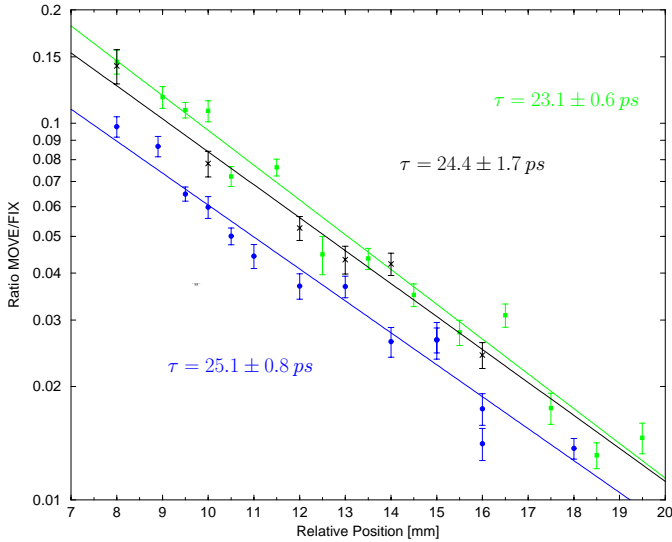


Figure 3: Measured decay curves of the 2^3P_0 state. The upper and the lower decay curves have been obtained for different normalizations detecting the x-rays in coincidence with He-like ions, while the decay curve in the middle has been obtained only detecting single x-rays.

2^3P_0	Theory		Experiment	
	[3]	[2]	this work	[7]
τ [ps]	24.66	23.66	23.9 ± 0.5	32 ± 4

Table 1: Comparison of the lifetime τ of the 2^3P_0 state between experiment and theory. Our experimental value is the weighted mean of all three decay curves.

sured, but only for one normalisation position. The error bars of the measured ratios are due to the statistical uncertainty at a 1σ confidence level. In order to extract the decay length l out of the decay curves, the data points have been fitted to a single exponential. With the extracted decay length l , the value for the speed of light c and the velocity of the ions β one can determine the lifetime in the laboratory frame:

$$\tau_{Lab} = \frac{1}{l\beta c}$$

This has to be transformed into the emitter frame, resulting in

$$\tau_{c.m.} = \frac{\tau_{Lab}}{\gamma}$$

for the lifetime of the 2^3P_0 state. The determined lifetimes of the different decay curves are also printed in Figure 3.

The given errors for the lifetimes are associated with the fitting procedure and are assumed to be the sole major contribution to the total experimental error. As one value overlaps with another value within the error bars, we took the weighted mean of all three values as a final result for the lifetime. The experimental results and the theoretical expectations are summarized in Table 1. Our final value agrees very well within the theoretical predictions. The results are only preliminary as the evaluation of the fine-structure splitting is still in progress.

One reason for the disagreement between the old and the new experiment may be the fact that the beam quality in the old experiment was very poor. As a consequence, the signal to back-

ground ratio was too low to get a reasonable result for the lifetime. In the new experiment the signal to background ratio has been enhanced roughly by a factor of four due to the improved beam quality. And now, even from detecting single x-rays one obtains a value for the lifetime, which agrees very well with the values that one obtains if one is using the coincidence technique.

Nevertheless, the reached accuracy of 2% looks promising concerning the planned experiment to measure the unquenched lifetime of the 2^3P_0 state in helium-like ^{238}U in the nuclear ground state from which the $n=2$ Lamb shift can be determined. Here the aim is to study the QED effects for the $2s$ -levels in a high- Z system with high accuracy.

References

- [1] G.W.F. Drake, Can. J. Phys. 66, 586 (1988)
- [2] P. Indelicato, F. Parente, R. Marrus, Phys. Rev. A40, 3505 (1989)
- [3] W.R. Johnson, D.R. Plante, J. Sapirstein, Adv. At. Mol. Phys. 35, 255 (1995)
- [4] P. Indelicato, B.B. Birkett, J.P. Briand, P. Charles, D.D. Dietrich, R. Marrus, A. Simionovici, Phys. Rev. Lett. 68, 1307 (1992)
- [5] B.B. Birkett, J.P. Briand, P. Charles, D.D. Dietrich, K. Finlayson, P. Indelicato, D. Liesen, R. Marrus, A. Simionovici, Phys. Rev. A47, R2454 (1993)
- [6] R. Marrus, A. Simionovici, P. Indelicato, D.D. Dietrich, P. Charles, J.P. Briand, K. Finlayson, F. Bosch, D. Liesen, F. Parente, Phys. Rev. Lett. 63, 502 (1989)
- [7] R. Marrus et al., GSI-95-1, 136 (1995)
- [8] H. Bräuning et al., GSI-2000-1, 91 (2000)
- [9] E. Berdermann, B.E. Fischer, M. Schlögl, H. Stelzer, B. Voss, GSI-Preprint-2000-09

Spectroscopy of Ly- α Lines at Storage Rings by Absorption-Edge Technique

M. Czanta¹, C. Strietzel², S. Toleikis¹, H.J. Besch², H.F. Beyer¹, F. Bosch¹, R. Deslattes⁵,
A. Gumberidze¹, P. Indelicato³, O. Klepper¹, C. Kozhuharov¹, A. Krämer¹, J. Lawall⁵, D. Liesen¹,
X. Ma¹, B. Manil³, N. Pavel², A. Simionovici⁴, M. Steck¹, T. Stöhlker¹, A.H. Walenta²

¹ GSI Darmstadt, Germany; ² Universität Siegen, Germany;

³ Université de Paris, France; ⁴ ESRF Grenoble, France; ⁵ NIST Gaithersburg, USA.

QED is very well tested in the case of light atoms. However, a test in the strong-field domain of highly charged heavy atoms with strongly pronounced higher order effects in $\alpha \cdot Z$ is still missing.

Sophisticated experiments have been devised to test QED in the high-Z region by the accurate determination of the ground-state Lambshift in hydrogenlike ions which recently has been calculated with an accuracy of the order of 10^{-5} of the ground-state binding energy of typically (60 – 130) keV [1]. The experiments are aimed to measure the Ly- α energies with comparable accuracy and therefore require instruments with high spectral resolution in the hard x-ray region. The absorption-edge technique fulfills this condition as has been demonstrated by a preliminary experiment [2, 3]. The experimental uncertainties of that “one-detector experiment” introduced by the Doppler-effect can be reduced by a measurement at several ion velocities β , x-ray observation angles Θ and absorbers.

The Doppler shift continuously depends on the ion velocity β and the angle of observation Θ while the energies of the K-edges discretely vary with the atomic number of the absorber. Since only a few fixed angles of observation at the gasjet target of the ESR are accessible, the number of suitable combinations of β , Θ and absorbers for a measurement on a certain ion is strictly limited.

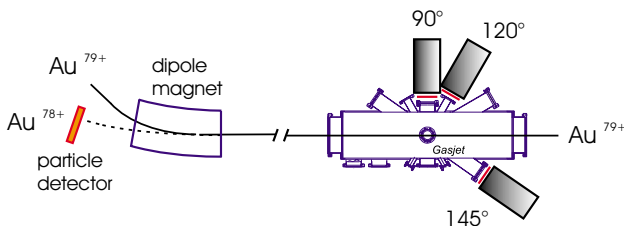


Figure 1: Experimental setup for the absorption-edge technique. Three position-sensitive drift chambers measure - in coincidence with downcharged ions - the intensity variations resulting from the shift of x-ray energies of H-like Au⁷⁸⁺ which are due to the angle-dependent Doppler-effect over the absorption edges of heavy absorbers.

In the case of hydrogenlike gold such a combination could be found for $\beta = 0.253$ and 0.4196 , $\Theta = 90^\circ$, 120° and 145° , and Sm, Tb, Ho, Tm, Lu and Ta as absorbers. The setup of an experiment performed in August 2000 is shown in Fig. 1. In this experiment, three position-sensitive drift-chambers [3, 4] were used for the measurement of the intensity variation of the Ly- α_2 line across the K-edges of the absorbers due to the angle-dependent Doppler shift. The line with the sharp peak at the right in

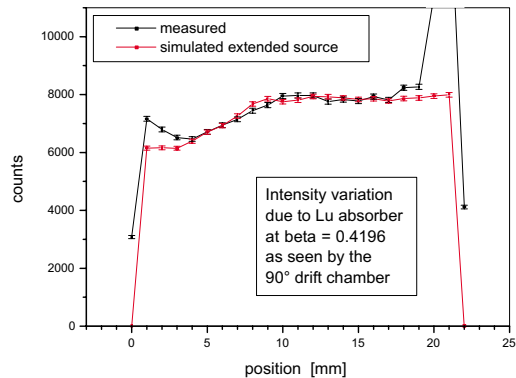


Figure 2: Measured and simulated intensity variation of the Ly- α_2 line along the Lu absorption edge at 90° emitted by H-like Au ions at $\beta = 0.4196$. The sharp peak results from the inner geometry of the drift chambers. The calculation corresponds to an extended source.

Fig. 2 shows the experimental result for $\beta = 0.4196$ and $\Theta = 90^\circ$ with Lu as absorber. Plotted is the observed intensity along the horizontal coordinate in the central plane of the detector, integrated over height and depth. The peak results from geometrical effects of the detector.

In order to analyse the experimental data, a program has been written which simulates the intensity variation of the detected photons. Here, the energies, widths and steps of the K-edges are fixed and the only free parameters are the observation angle Θ , the size of the emitting volume and the photon energy in the rest frame.

The line without sharp peaks in Fig. 2 shows preliminary results of the simulations for a 2 mm in diameter and 5 mm long emitting volume assuming $\Theta = 90^\circ$ and the theoretical energy of the Ly- α_2 transition [1] in comparison with the experimental data. Since the width of the observed absorption edge is sensitive to the spatial distribution of the emitting volume, it turns out that the extended source is close to the chosen values. The final results will be obtained from a combined fit of the simulations to the experimental data for all K-edges observed.

References

- [1] Th. Beier et al., Phys. Lett. A 236, 329 (1997)
- [2] C. Strietzel et al., GSI Scient. Rep. 1999, p.208
- [3] C. Strietzel, Thesis, Universität Siegen, 2000
- [4] M. Czanta et al., GSI Scient. Rep. 1999, p.207

Radiative Electron Capture into the K- and L-shell of H-, He-, and Li-Like Uranium Ions at Relativistic Energies

G. Bednarz¹, A. Warczak¹, D. Sierpowski¹, Th. Stöhlker², F. Bosch², A. Gumberidze², S. Hagmann²,
C. Kozuharov², D. Liesen², X. Ma², P.H. Mokler², T. Ludziejewski³, Z. Stachura⁴

¹ IFUJ-Cracow (Poland), ² GSI-Darmstadt (Germany), ³ INS-Swierk (Poland), ⁴ INP-Cracow (Poland)

Radiative electron capture (REC) is the most important channel for charge exchange in collisions of highly charged ions with light target atoms. As, in addition, the process is the time reversal of photoionization, its investigation opened new possibilities for advanced studies of radiation-matter interaction [1]. In particular, angular distribution of REC photons is a very sensitive probe of relativistic effects in strong fields of heavy ions. Here, magnetic spin-flip transitions were observed, for the first time, in fast collisions of bare U-ions [2] with low Z-ions. Even, at very low projectile velocities, corresponding to photoionization close to the threshold, the presence of these transitions was confirmed as well [3].

We report the experimental study of the angular distributions of photons for REC into the K-shell of H-like and into the L-shell of H-, He- and Li-like uranium ions. The main goal was to observe the role of spectator electrons in the heavy projectile in order to reveal possible electron-electron correlations.

The experiment was performed at the ESR storage ring at GSI-Darmstadt. The U^{91+} -, U^{90+} - and U^{89+} -ions at an energy of 216 MeV/u colliding with N_2 -target were used. X-rays emitted from the active target area were detected simultaneously at 13°, 35°, 60°, 90°, 120° and 150° with respect to the beam axis. At all the angles Ge(i) detectors equipped with x-ray collimator slits (except for 13°) were used. The collimator dimensions allowed us to resolve the splitting of the $K\alpha$ transitions into the $K\alpha_1$ and $K\alpha_2$ components. At 13°, a Ge(i) detector with four independent segments, each furnished with an individual readout, was installed on a moveable support. After passing through the target the beam was charge state analysed in the next dipole magnet. Down- and up-charged U-ions were registered (for the study of capture and ionisation processes) with position-sensitive particle detectors located in the inner and outer part of the storage ring. In the following, preliminary results concerning electron capture are presented and discussed only.

Fig.1 shows a typical x-ray spectrum observed at 90° for U^{91+} -ions associated with capture of one electron. The broad structures arise from REC into the projectile K-, L- and M-shells. The line-widths are dominated by the Compton profile of the target electrons. Electron capture into excited states (L, M and higher shells) leads, via cascades, to the

characteristic $K\alpha$ - and $K\beta$ -transitions, clearly seen in the spectra.

All the x-ray spectra were first energy calibrated and corrected for random events and for detection efficiency. Then, the yields of K- and L-REC photons were determined via special fits to the experimental spectra. Simultaneously, the intensities of $K\alpha_2$ -lines ($U^{91+} \rightarrow N_2$) were extracted. Assuming, that the $K\alpha_2$ -line (similar to the $Ly\alpha_2$ -line) is isotropic in the emitter system, all the angular distributions (U^{91+} , U^{90+} , $U^{89+} \rightarrow N_2$) for K- and L-REC were normalised relative to its intensity pattern in the laboratory frame.

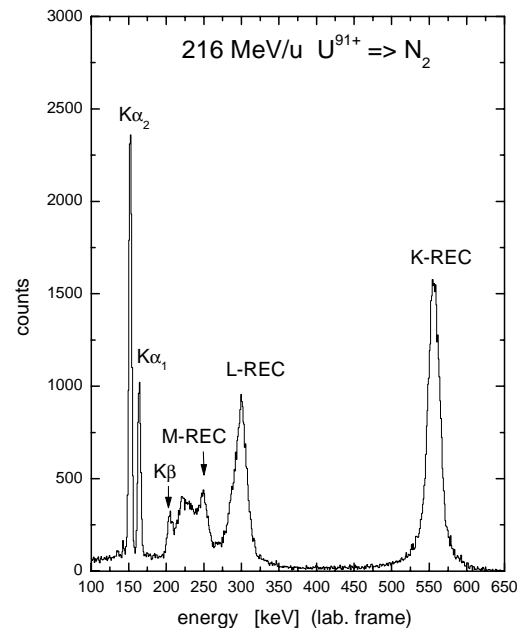


Fig.1 X-ray spectrum associated with one-electron capture (corrected for random events and detection efficiency) observed at an observation angle of 90°.

In Fig.2, the measured differential cross section for REC into the K-shell of 216 MeV/u U^{91+} -ions (present experiment) and 310 MeV/u U^{92+} -ions [2] are plotted as a function of the laboratory observation angle and compared with predictions (for $U^{92+} \rightarrow N_2$) based on rigorous relativistic calculations [4]. (The data obtained in the present experiment for 120° are still under evaluation and are therefore not displayed.)

All the experimental and theoretical cross sections were normalised to an arbitrary value at 90° . Fig.2 shows that the shape of the angular distribution is almost unchanged when comparing the results for bare and H-like U-ions. The experimental data are in accordance with a fully relativistic theoretical description (solid line). The REC emission pattern deviates considerably from symmetry around 90° (compare dashed-line displaying a $\sin^2\theta_{lab}$ distribution). Nonvanishing cross sections close to 0° point to the occurrence of magnetic (spin-flip) transitions for REC into high-Z projectiles.

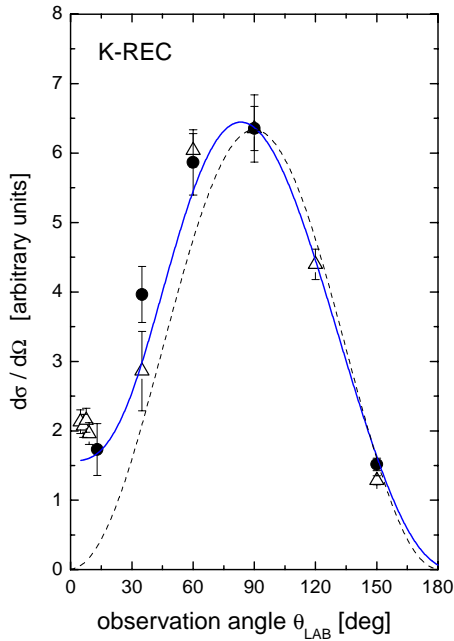


Fig.2 K-REC differential cross sections for 216 MeV/u $U^{91+} \rightarrow N_2$ (circles) and for 310 MeV/u $U^{92+} \rightarrow N_2$ (triangles); dashed-line – $\sin^2\theta_{lab}$ distribution, solid-line – relativistic predictions for bare U-ions [4].

The differential cross sections for L-REC into U^{91+} -, U^{90+} - and U^{89+} -ions are presented in Fig.3a, 3b, 3c, respectively, along with theoretical calculations for the different subshells [4]. Similar to the K-REC, the photons observed at 0° and 180° angles present a clear signature of magnetic transitions. A basic feature of all the angular distributions displayed in Fig.3 is the asymmetry between the forward and the backward photon emission. The main contribution for H-like (Fig.3a) and He-like U-ions (Fig.3b) arises from the capture into the 2s-shell (dotted-line in Fig.3a) which has a pronounced maximum at the forward direction. Contributions from the 2p-shells (dashed-line: $2p_{1/2}$, dashed-dotted line: $2p_{3/2}$) reach their maximum at backward angles and do not compensate this forward peaking. In the case of $U^{89+} \rightarrow N_2$ system (Fig.3c) the emission pattern is shifted into backward direction due to the partially blocked contribution from the 2s-shell. Here, again the experimental data agree well with

theoretical predictions taking into account only one electron present initially in the 2s-shell of U^{89+} (compare dashed-line in Fig. 3c. for one initial 2s vacancy and the full line for two initial 2s vacancies). In summary, we measured the angular distributions of K- and L-REC into H-, He-, and Li-like U-ions at an energy of 216 MeV/u. They are found to be asymmetric and more pronounced at forward directions. The emission pattern for K-REC stays unchanged for bare and H-like U-ions. One electron present in the L-shell of the projectile (U^{89+}) shifts the photon emission into backward direction. The experimental data provide an excellent agreement with rigorous relativistic predictions.

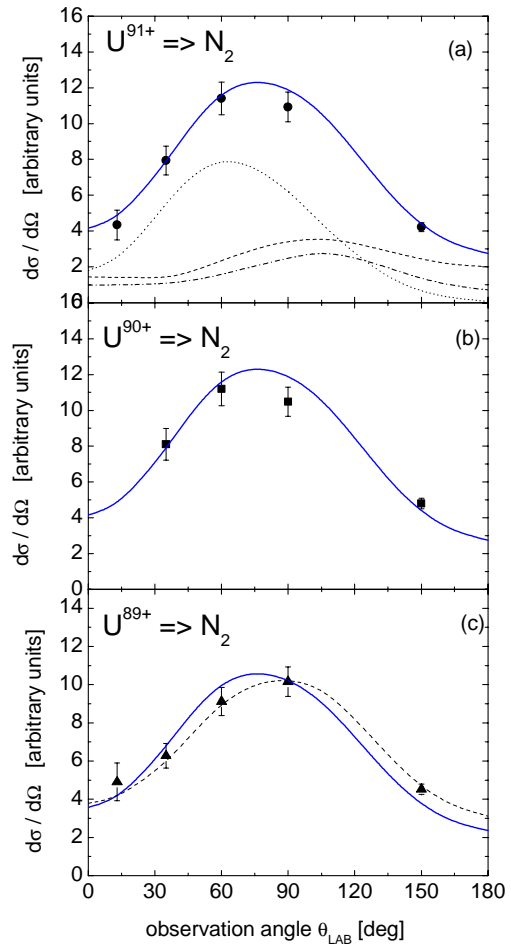


Fig.3 Differential cross sections for capture into the L-shell of U^{91+} (a), U^{90+} (b), U^{89+} (c). (a) dotted-line: capture into the $2s_{1/2}$ -shell, dashed-line: $2p_{1/2}$ -shell, dot-dashed-line: $2p_{3/2}$ -shell; (c) dashed-line – see text. All solid lines refer to the summed contributions for completely empty $2s_{1/2}$ -, $2p_{1/2}$ -, and $2p_{3/2}$ -subshells (relativistic predictions [4]).

References

- [1] Th. Stöhlker et al., Com. At. Mol. Phys. **33**, 271 (1997).
- [2] Th. Stöhlker et al., Phys. Rev. Lett. **82**, 3232 (1999).
- [3] Th. Stöhlker et al., Phys. Rev. Lett. **86**, 983 (2001).
- [4] A. Ichihara et al., Phys. Rev. A **49**, 1875 (1994).

State-Selective Electron Capture Studied for U^{90+} Ions in Collisions with Gaseous Targets

X. Ma^{1,2}, Th. Stöhlker^{1,3}, F. Bosch¹, O. Brinzaescu¹, S. Fritzsche⁴,
C. Kozhuharov¹, P.H. Mokler¹, T. Ludziejewski⁵, A. Warczak⁶

¹GSI-Darmstadt, Germany; ²IMP, Lanzhou, China; ³IKF, Univ. of Frankfurt, Germany; ⁴Univ. Kassel, Germany

⁵INS, Świerk, Poland; ⁶Institute of Physics and Jagiellonian University, Cracow, Poland.

In relativistic collisions involving high-Z projectiles and heavy target atoms, non-radiative electron capture (NRC) is a very important charge exchange process [1], a process mediated by three-body interaction. In general, a precise theoretical treatment of this process is very difficult to achieve since the Coulomb field of the fast moving projectile leads to distortions of the atomic target wave functions even at infinite distances. For high-Z ions and relativistic energies the experimental information about NRC is restricted to total cross sections which are quite insensitive to the details of this process. An experiment aiming at a study of state-selective electron capture was conducted at the gas-jet area of the ESR, by utilizing the spectroscopy of projectile x-ray transitions following electron capture into excited projectile states. This method benefits in particular from the large fine structure splitting present in such heavy ion systems. In the experiment, the Balmer radiation produced by electron capture in collisions of 223 MeV/u U^{90+} ions on N_2 , Ar, Kr, and Xe targets have been measured in coincidence with the down-charged uranium ions (here *Balmer* transition refers to the transitions from higher levels to $n=2$ states). The recorded x-ray spectra are shown in figure 1. As the target varies from light to heavy atoms, the relative intensities of the *Balmer* lines exhibit a significant change. This feature already indicates a strong influence of the target charge on the relative population of the various (n, l, j) projectile sublevels by electron capture.

The intensity pattern of the multitude of well-resolved *Balmer* transitions was used to obtain the j -selective cross section data as a function of target Z_T . For this goal a spectrum analysis and simulation code has been developed where electron cascades originating from states up to $n=40$ are considered. The latter was accomplished by using the individual decay rates and transition energies of all states involved. In the spectra simulation, both the NRC and the radiative electron capture (REC) were taken into account. The CDW theory was used to calculate the NRC cross sections. To obtain experimental information on the j -sensitive population for electron capture, a fit to the measured spectra was carried out by setting the relative cross sections as fitting parameters. From this procedure, the information on relative populations to the different j -sublevels has been deduced [2]. For N_2 , where the cross sections for REC are a factor of 10 larger than for NRC, good agreement with theory is obtained. Here, the captured electrons mainly populate the s and p states where the $s_{1/2}$ levels are more favored which is in agreement with REC theory and the j -substate distribution behaves non-statistically. For the heavier targets (Ar, Kr, and Xe), NRC is the most important capture

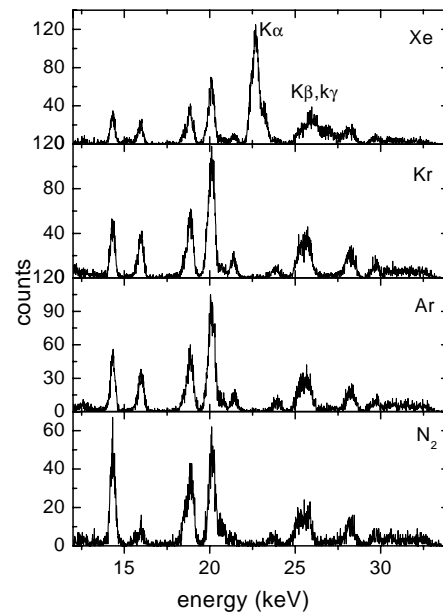


Figure 1: *Balmer* spectra measured in 223 MeV/u U^{90+} impinging on N_2 , Ar, Kr, and Xe targets. For the case of Xe, also characteristic target transitions ($K\alpha, K\beta, K\gamma$) are observed.

process. This process leads to a n, l, j -distribution which differs markedly from the one observed in the case of the N_2 -target (REC). Here, our data analysis shows that NRC seems to favor the population of states with angular momentum $l=1$ which appears to be only in rough agreement with the CDW approach applied. The discrepancies between our data and the latter approach are in particular evident with respect to the j -dependency. For CDW a statistical j -distribution had to be assumed since we are dealing with a non-relativistic theory. For the case of high-Z projectiles, however, this assumption is questionable (see e.g. Ichihara[3]). The systematic deviations between the experimental data and the theoretical calculations for the j -subshell cross sections indicate that a relativistic approach is needed for an appropriate description of NRC in the high-Z domain.

References

- [1] J. Eichler and W. E. Meyerhof, Relativistic Atomic Collisions (Academic press, San Diego, 1995).
- [2] X. Ma et al., Physica Scripta (in print).
- [3] A. Ichihara, T. Shirai, and J. Eichler, At. Data and Nucl. Data Tab. 55 63 (1993).

Magnetic Sublevel Population Studied for H- and He-Like Uranium in Relativistic Collisions with Low-Z Targets

A. Gumberidze¹, Th. Stöhlker^{1,2}, G. Bednarz³, F. Bosch¹, S. Fritzsche⁴, S. Hagmann⁵, D.C. Ionescu^{1,6}, C. Kozhuharov¹, O. Klepper¹, A. Krämer^{1,2}, D. Liesen¹, X. Ma^{1,7}, R. Mann¹, P.H. Mokler¹, D. Sierpowski³, Z. Stachura³, M. Steck¹ and A. Warczak³

¹GSI-Darmstadt, Germany; ²IKF, Univ. of Frankfurt, Germany; ³Institute of Physics, Cracow University, Poland;

⁴Univ. of Kassel, Germany; ⁵Kansas State University, Kansas, USA; ⁶TU Dresden, Germany; ⁷IMP, Lanzhou, China.

In contrast to ionization, the experimental information about Coulomb excitation of one- and few-electron projectiles occurring in relativistic atomic collisions is very scarce. The lack of data must be attributed to the experimental difficulties which arise from the fact that excitation is not accompanied by projectile charge exchange. As a consequence, this process can only be studied in single pass experiments by measuring the photon production in coincidence with primary beams of low intensity. Indeed, this technique was applied in the first experimental study of projectile K -shell excitation for high- Z ions [1, 2]. Although this experimental study already elucidated the sensitive dependence of the excitation process on the details of the relativistic bound state wave-functions in the theoretical description, the experimental results suffered from counting statistics. Very recently, an alternative experimental approach has been introduced at the storage ring ESR. Here, the formation of excited states in Au^{78+} in relativistic collisions with an Ar target by Coulomb excitation has been studied by detecting the projectile x-ray emission in anti-coincidence with charge exchange [3]. By using this technique we now started to extend our earlier investigations to a more detailed angular differential study for the collision systems U^{91+} , $\text{U}^{90+} \rightarrow \text{N}_2$ at 217 MeV/u. For x-ray detection, observation angles in the range between $\approx 10^\circ$ and 150° were used at the atomic physics photon detection chamber of the internal target of the ESR (for details see Ref. [4]).

In the experiment, the projectile x-ray emission was measured in coincidence with down-charged ions as well as in a single mode, i.e. without any coincidence requirement. As a representative example we depict in Fig. 1 x-ray spectra recorded for $\text{U}^{91+} \rightarrow \text{N}_2$ collisions at the forward angle of close to 10° . In the spectra, the transitions arising from electron capture ($K\alpha$ transitions in He-like uranium) and these from excitation ($\text{Ly}\alpha$ transitions in H-like uranium) can clearly be distinguished by both the transition energies as well as by the coincidence requirement. Indeed, no $K\alpha$ transitions are observed in the anti-coincidence spectrum. This also proves that the MWPC detector used for particle detection operates with a detection efficiency very close to 100%.

In the following we concentrate on the formation of magnetic-sublevels by Coulomb excitation as well as by electron capture. Information about this topic can be obtained from the study of the angular distribution of the photons associated with these processes. For the particular case of **E1** transitions, the photon angular correlation has the form:

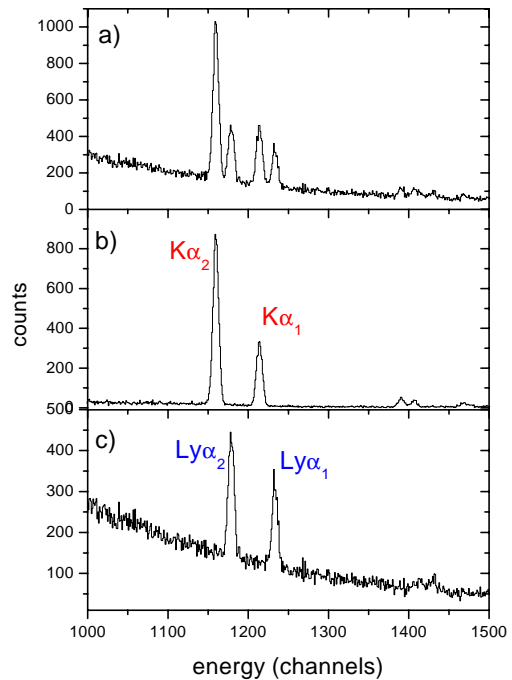


Figure 1: X-ray spectra recorded for 217 MeV/u $\text{U}^{91+} \rightarrow \text{N}_2$ collisions at the forward angle of close to 10° (a: total emission spectrum without coincidence requirement; b: photons in coincidence with electron capture; c: photons in anti-coincidence with electron capture).

$$W(\theta) = A_0 + A_2 P_2(\cos \theta) \propto 1 + \beta_{20} (1 - \frac{3}{2} \sin^2 \theta). \quad (1)$$

Here θ is the angle between the de-excitation photon and the axis defined by the projectile motion (projectile frame) while P_2 is the second-order Legendre polynomial. The angular correlation is completely determined by the anisotropy coefficient β_{20} . In general, $W(\theta)$ is symmetric about 90° in the projectile frame and isotropic if the intermediate state has $j_n = \frac{1}{2}$ as it is the case for the $\text{Ly}\alpha_2$ ($2p_{1/2} \rightarrow 1s_{1/2}$) transition. For the particular case of the $2p_{3/2}$ transition, however, one may also determine β_{20} from the alignment \mathcal{A}_2 of the state which is defined as

$$\mathcal{A}_2 = \frac{\sigma(\frac{3}{2}, \pm\frac{3}{2}) - \sigma(\frac{3}{2}, \pm\frac{1}{2})}{\sigma(\frac{3}{2}, \pm\frac{3}{2}) + \sigma(\frac{3}{2}, \pm\frac{1}{2})} = \frac{1}{\alpha} \beta_{20}, \quad (2)$$

where $\sigma(j = \frac{3}{2}, \mu)$ is the population of the magnetic substate with $\mu = \pm\frac{1}{2}, \pm\frac{3}{2}$. For the $2p_{3/2} \rightarrow 1s_{1/2}$ transition, $\alpha = \frac{1}{2}$. Quite similar expressions can be found

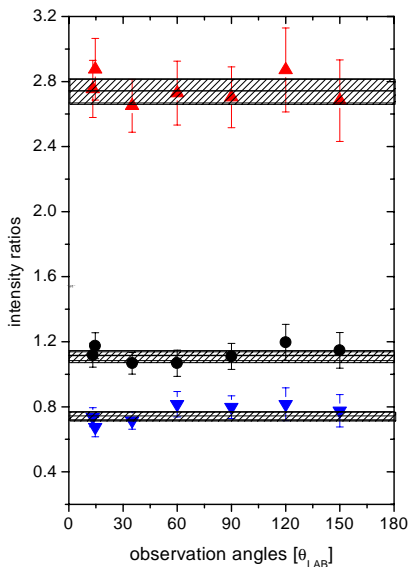


Figure 2: The intensities of $K\alpha_2$ - (up-triangles), $K\alpha_1$ - (solid circles), $Ly\alpha_1$ -transitions (down-triangles) normalized to the $Ly\alpha_2$ line as function of observation angle. The experimental data were recorded for $U^{91+} \rightarrow N_2$ collisions at the energy of 217 MeV/u. The full lines refer to the corresponding mean values and the shaded areas give the associated uncertainties.

for the case of the **E1** decay of the $[1s_{1/2}, 2p_{1/2}]^3P_1$ and the $[1s_{1/2}, 2p_{3/2}]^1P_1$ states in the He-like systems. Here, however, magnetic sublevels with the quantum numbers of $\mu_{J=1} = 0, \pm 1$ must be considered.

In our current experiment we strongly profited from the fact that the $Ly\alpha_2$ transition arising from the decay of the $2s_{1/2}, 2p_{1/2}$ levels is known to be precisely isotropic. Consequently, it provides an ideal tool to measure a possible anisotropy of the close spaced $Ly\alpha_1$ or $K\alpha$ transitions. In Fig. 2 the preliminary results for the emission pattern of the $Ly\alpha_1$ and the $K\alpha$ transitions are shown, normalized to the $Ly\alpha_2$ intensity. In all cases no alignment is observed and the magnetic sublevels are therefore populated statistically. In the case of the $Ly\alpha_1$ transition ($2p_{3/2} \rightarrow 1s_{1/2}$) induced by excitation this finding seems to be in agreement with theoretical predictions [5]. However, the isotropy of the $K\alpha_1$ emission [$1s_{1/2}, 2p_{3/2}]^1P_1, ^3P_2$, which is caused by electron capture, is in contradiction to former observations and theoretical predictions for capture into bare uranium where a strong alignment of the $2p_{3/2}$ state was observed [6]. This surprising result may point to the importance of electron-electron interaction for the emission characteristic of excited levels in high-Z He-like ions. But we have also to emphasize that the decay of two levels (**E1** decay for 1P_1 , **M2** decay for 3P_2) contribute to the $K\alpha_1$ transition which cannot get resolved in our experiment. Since both transitions exhibit different angular distributions this may wipe out a distinctive anisotropy of the $K\alpha_1$ emission. Currently this topic is subject of detailed theoretical investigations.

Also for K-shell excitation we observed a markedly difference between the H- and the He-like species. In Fig. 3,

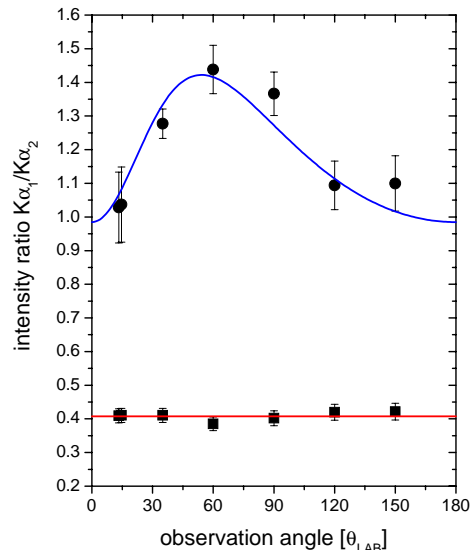


Figure 3: $K\alpha_1/K\alpha_2$ intensity ratio (solid circles) as observed for K-shell excitation of He-like uranium in collisions with N_2 at 217 MeV/u. The solid line refers to a least square fit of Eq. (1) to the experimental data including all required relativistic transformations. For comparison the corresponding intensity ratio (solid squares) as measured for capture into H-like uranium is shown.

the $K\alpha_1/K\alpha_2$ intensity ratio, as measured for K-shell excitation of He-like uranium in 217 MeV/u $U^{91+} \rightarrow N_2$ collisions, is plotted as a function of the observation angle. For comparison the corresponding intensity ratio (solid squares) as measured for capture into H-like uranium is shown in addition. In contrast to electron capture, the data for excitation exhibit a pronounced deviation from a constant intensity ratio. Note, that for the case of K-shell excitation of high-Z He-like ions, only the $[1s_{1/2}, 2p_{3/2}]^1P_1$ contributes to the $K\alpha_1$ transition whereas the $K\alpha_2$ intensity arises from the decay of the $[1s_{1/2}, 2p_{1/2}]^3P_1$ level only. In both cases an alignment of the different sublevels is possible. At present, it has not been clarified which of both states causes the observed anisotropic intensity ratio. However, at the current state of data analysis there are strong indications of a positive alignment of the $[1s_{1/2}, 2p_{1/2}]^3P_1$ level. This means that the magnetic sublevels with $\mu = \pm 1$ are preferably populated in the collision.

References

- [1] Th. Stöhlker et al., Phys. Rev. A **57**, 845 (1998); Phys. Lett. A **238**, 43 (1998).
- [2] T. Ludziejewski et al., Phys. Rev. A **61**, 052706-1 (2000).
- [3] A. Krämer et al., Physica Scripta T80, 424 (1999).
- [4] Th. Stöhlker et al., in: "X-Ray and Inner Shell Processes", AIP Conference Proc. 506, 389 (2000).
- [5] D.C. Ionescu and Th. Stöhlker, contribution to this report.
- [6] Th. Stöhlker et al., Phys. Rev. Lett. **79**, 3270 (1997).

Projectile K-Shell Vacancy Production in $U^{89+} \rightarrow N_2$ Collisions: Selective Population of the 2s-States in He-Like Uranium

Th. Stöhlker^{1,2}, A. Gumberidze¹, G. Bednarz³, F. Bosch¹, S. Fritzsche⁴, S. Hagmann⁵,
D.C. Ionescu^{1,6}, C. Kozhuharov¹, A. Krämer^{1,2}, D. Liesen¹, X. Ma^{1,7}, R. Mann¹,
P.H. Mokler¹, D. Sierpowski³, Z. Stachura³, M. Steck¹, and A. Warczak³

¹GSI-Darmstadt, Germany; ²IKF, Univ. of Frankfurt, Germany; ³Institute of Physics, Cracow University, Poland;

⁴Univ. of Kassel, Germany; ⁵Kansas State University, Kansas, USA; ⁶TU Dresden, Germany; ⁷IMP, Lanzhou, China.

Until now, atomic physics experiments at the ESR storage ring focused on initially bare and hydrogen-like ions. However, there is an increasing demand to extend the range of possible structure and collision studies to heavy high-Z multi-electron systems such as helium-, lithium-, or beryllium-like ions. To accomplish the storage of intense heavy few-electron systems even at the highest beam energies possible at the ESR, thin carbon stripper foils are now available in the beam transfer line between SIS and ESR. In contrast to the commonly used copper stripper targets, carbon foils guarantee a strong yield enhancement for heavy multi-electron ions (see. Fig. 1). Very recently, this new possibility for atomic physics experiments has been exploited by injecting intense SIS beams of lithium-like uranium into the ESR at an energy of 217 MeV/u. In this experiment, projectile x-ray emission arising from collisions with a N_2 target was measured by intrinsic germanium detectors in coincidence with down-charged or up-charged ions, i.e. ions having captured (U^{88+}) or lost (U^{90+}) one-electron in the collision. For a detailed description of this set-up we refer to Ref. [1]. In the following we concentrate on the process of K-shell ionization. In Fig. 2 the x-ray spectrum observed at an forward angle of $\approx 10^\circ$ in coincidence with electron-loss is depicted. The spectrum is entirely governed by an intense single $L \rightarrow K$ ($K\alpha_2$) transition and a broad continuum distribution. Since we are dealing with He-like uranium produced by K-shell vacancy production of the Li-like species, the broad continuum can be explained by the two-photon decay ($2E1$) of the $[1s_{1/2}, 2s_{1/2}]^1S_0$ level. Consequently, the single $K\alpha$ transition observed arises exclusively from the $M1$ decay of the $[1s_{1/2}, 2s_{1/2}]^3S_1$ state. To the best of our knowledge, no other process occurring in ion-atom collisions is known with such a high state selectivity. This also means that the 2s-electron stays passive during a collision leading to K-shell ionization because no decay from the neighbouring excited p-states is observed (see level scheme inserted in Fig. 2). This unexpected and surprising finding is currently subject of theoretical studies.

References

- [1] Th. Stöhlker et al., in: "X-Ray and Inner Shell Processes", AIP Conference Proc. 506, 389 (2000).
- [2] C. Scheidenberger et al., Nuclear Instr. and Methods B **142**, 441 (1998).

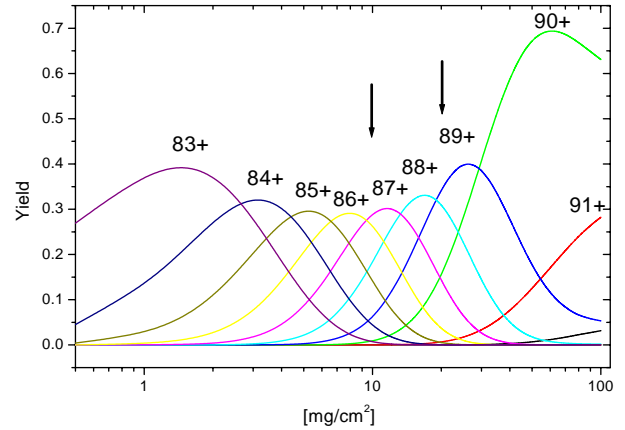


Figure 1: Calculated charge state evolution as function of target thickness for uranium ions traversing through a carbon foil at an energy of 300 MeV/u. For the calculation the program GLOBAL has been used [2]. The arrows mark the target thickness of the stripper targets installed.

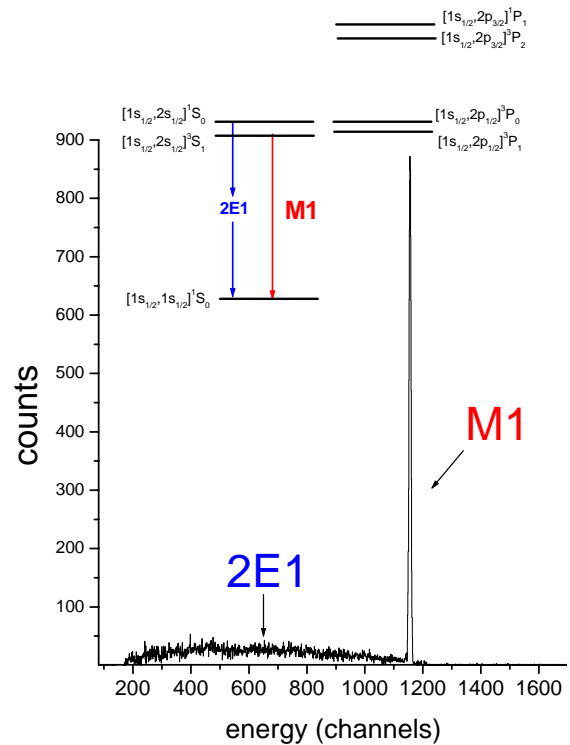


Figure 2: X-ray spectrum measured in coincidence with electron loss for $U^{89+} \rightarrow N_2$ collisions at 217 MeV/u. In the upper part, the level scheme of He-like uranium illustrates the origin of the observed photon emission.

Resonant Transfer and Excitation for H-like U Ions: A Case Study for Electron-Electron Interaction at Strong Central Fields

X. Ma^{1,2}, P.H. Mokler¹, G. Bednarz³, F. Bosch¹, A. Gumberidze¹, S. Hagmann¹, C. Kozhuharov¹, D. Liesen¹, U. Popp¹, D. Sierpowski³, Z. Stachura⁴, Th. Stöhlker¹, S. Tashenov⁵, S. Toleikis¹, A. Warczak³, Y. Zou⁶
¹GSI, Darmstadt, Germany; ²IMP, Lanzhou, China; ³Jagiellonian University, Cracow, Poland; ⁴IFJ, Cracow, Poland; ⁵State University Moscow, Russia; ⁶Jiaotong University, Shanghai, China.

Structure and dynamics for the heaviest atomic systems differ significantly from those of lighter ions due to the extremely strong central fields at the high atomic numbers Z . In particular relativistic effects are essential. There, for instance, the electron-electron interaction is governed beyond the Coulomb forces by the current or magnetic interactions (Breit term) which may change the corresponding Auger emission drastically [1]. Collisions of highly-charged heavy ions with quasi-free electrons from light target atoms provide a unique tool to investigate the electron-electron interaction in the relativistic domain via resonant capture and excitation. This resonant transfer and excitation (RTE) is the time reversal of the Auger process and leads first to a doubly excited state. For high- Z ions the intermediate doubly excited state stabilizes by x-ray emission due to the high radiative rates, cf. [2] [3].

The electron-electron interaction can be studied in an unperturbed manner for incoming H-like ions interacting with one target electron. Therefore, we have investigated this pure case at the ESR gas target for the heaviest possible system, for H-like U^{91+} projectiles colliding with hydrogen. For hydrogen as gas target the momentum distribution of the quasi-free electron determining the RTE resonance width (Compton profile) is the smallest possible. Fig. 1 shows the three $KL_jL_{j'}$ resonances (top) where one electron is captured into a $L_{j'}$ level and the K electron is excited resonantly to a L_j level – with $j, j' = 1/2, 3/2$ – and the following radiative decay modes (bottom). Satellite and hypersatellite x-ray lines (one and two initial K vacancies) can be separated by the Ge(i) x-ray detectors used.

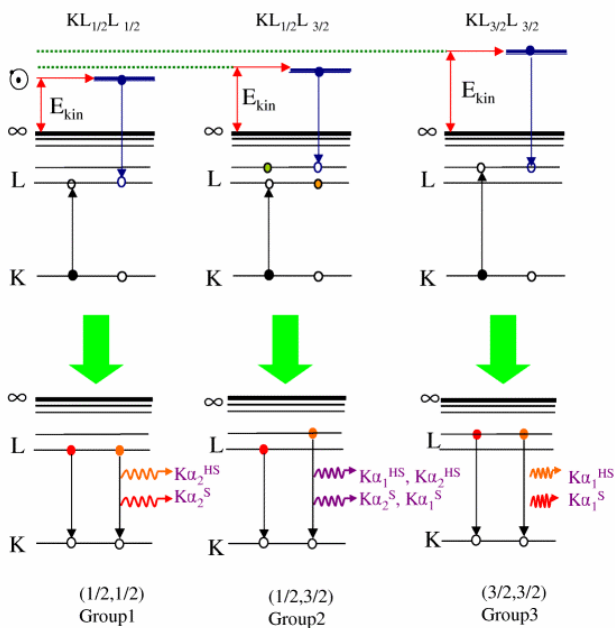


Fig.1: $KL_jL_{j'}$ RTE resonances and their radiative decays for incoming H-like U^{91+} ions.

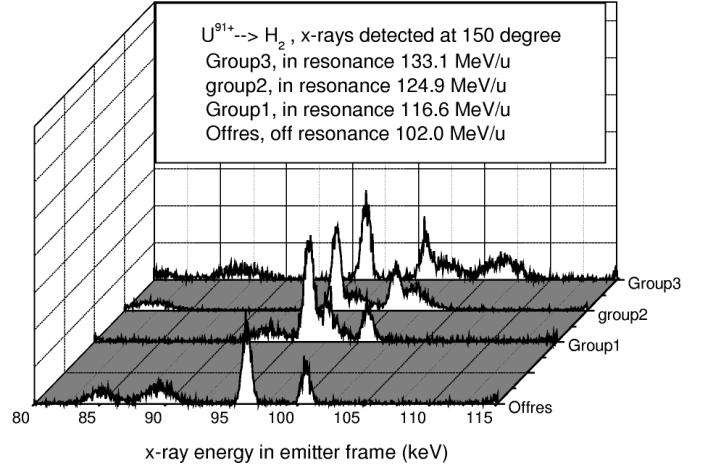


Fig. 2: X-ray spectra observed at 150° for U^{91+} - H collisions.

We have determined the x-ray emission pattern induced by U^{91+} - H collisions using six different observation angles (from $\approx 12^\circ$ to 150°) for the three RTE resonance maxima and for one off-resonance ion energy, cf. Fig. 2. For the off-resonance data at 102 MeV/u ion energy we find in the x-ray spectrum the L_j - REC lines with $j = 3/2$ and $1/2$ (at ≈ 85 and 89 keV) and the subsequent $K\alpha_2$ and $K\alpha_1$ cascade lines (at ≈ 96 and 100 keV). With higher ion energies the REC lines shift correspondingly to higher x-ray energies. At the $KL_{1/2}L_{1/2}$ resonance – group 1 at 116.6 MeV/u in Fig. 2 – the $L_{1/2}$ -REC line coincides with the $K\alpha_2^H$ hypersatellite line caused totally by RTE (at ≈ 97 keV). At 124.9 MeV/u, the $KL_{1/2}L_{3/2}$ -RTE resonance (group 2), both L_j -REC lines coincides with both the $K\alpha_i^H$ hypersatellites each. Finally, for the $KL_{3/2}L_{3/2}$ resonance at 133.1 MeV/u (group 3) the $L_{3/2}$ -REC line (at ≈ 102 keV) coincides with the $K\alpha_1^H$ hypersatellite line; the $L_{1/2}$ -REC line (at ≈ 106 keV) is here already beyond the region of interest.

The data are presently being evaluated in order to extract both total rate coefficients for the electron-electron interaction at strong fields and to get the angular distributions of the x-ray emission. From the emission patterns the j dependent level population of the doubly excited intermediate states can be deduced giving detailed insight into the electron-electron interaction mechanism in the relativistic domain. Calculations for this system are presently being performed by the theory group in Giessen, cf. [4].

References

- [1] P. Zimmerer et al., Phys. Lett. A148 (1990) 457
- [2] T. Kandler et al., Phys. Lett. A204 (1995) 274
- [3] P.H. Mokler et al., Physica Scripta T73 (1997) 247
- [4] M. Gail et al., J. Phys. B31 (1998) 4645

Measurement of Photorecombination of Highly Charged Ions at Low Relative Energies

C. Brandau^a, T. Bartsch^a, K. Beckert^b, S. Böhm^a, C. Böhme^a, F. Bosch^b, B. Franzke^b, N. Grün^c, A. Hoffknecht^a, H. Knopp^a, S. Kieslich^a, C. Kozhuharov^b, A. Krämer^b, P.H. Mokler^b, A. Müller^a, F. Nolden^b, W. Scheid^c, S. Schippers^a, W. Shi^a, Z. Stachura^d, M. Steck^b, T. Steih^c, T. Stöhlker^b,

^aInstitut für Kernphysik, Justus-Liebig-Universität, 35392 Gießen

^bGesellschaft für Schwerionenforschung (GSI), 64291 Darmstadt

^cInstitut für Theoretische Physik, Justus-Liebig-Universität, 35392 Gießen

^dInstytut Fizyki Jądrowej, 31-342 Kraków, Poland

In the ongoing work on photorecombination (PR) measurements at the electron cooler of the ESR new results have been obtained during the last year. PR is the capture of a free electron under emission of one or more photons. It is usually described as two different processes, radiative recombination (RR) and dielectronic recombination (DR).

The interest in RR, which is the direct path of PR (time-inverse photoeffect), is mainly driven by the puzzling "rate enhancement phenomenon" at very low relative energies between electrons and ions. On the other hand in resonant DR, the free electron is captured radiationless by the ion (inverse to autoionisation), and a doubly excited compound system is formed. If the intermediate state decays under emission of a photon DR is completed. Therefore, investigations of DR provide insight into the atomic structure of the very heavy highly charged ions under study at the GSI.

RR measurements of U⁹²⁺

For relative energies between electrons and ions above 0.01-0.1 eV up to very high energies the measured rate coefficient for RR can be described by the dipole approximation within a non-relativistic treatment. However, at very low energies recombination rates exceed the predictions by factors of 1.6 for light ions and up to a factor of 5.2 for heavier bare species. For multi-charged complex ions even higher enhancement factors have been found, which could partly be explained by low energy DR-resonances. Of course, for bare ions recombination can not proceed via DR. As a measure for the enhancement an excess rate $\Delta\alpha = \alpha_{exp} - \alpha_{theo}$ is defined. While the enhancement turns out not to be influenced by the electron target density, $\Delta\alpha$ is found to scale with the temperatures of the electron beam like $T_{\perp}^{-1/2}$ and $T_{\parallel}^{-1/2}$. The dependence of the rate enhancement on the strength of the magnetic field used to guide the electron beam inside the cooler is even more puzzling than the enhancement itself: An increase of the enhancement with increasing magnetic field is commonly found at all storage rings. In addition, for very heavy ions at high ion energies, and hence at high electron energies, nearly periodic oscillations of the RR rate coefficient in dependence of the magnetic field strength have been observed at the ESR [1, 2]. So far, for very heavy bare ions ($Z > 18$) detailed investigations of the enhancement have only been performed with Bi⁸³⁺ [2]. Recently, measurements with 297.1 MeV/u U⁹²⁺ ions have been carried out at the ESR. The recombined ions have been detected with a position sensitive counter. This additional diagnostics allows one to monitor the ion beam properties during the measurement. It turned out that the size of the ion beam changes in the horizontal (x-) direction while for the size in the vertical direction no changes under variation of the guiding field

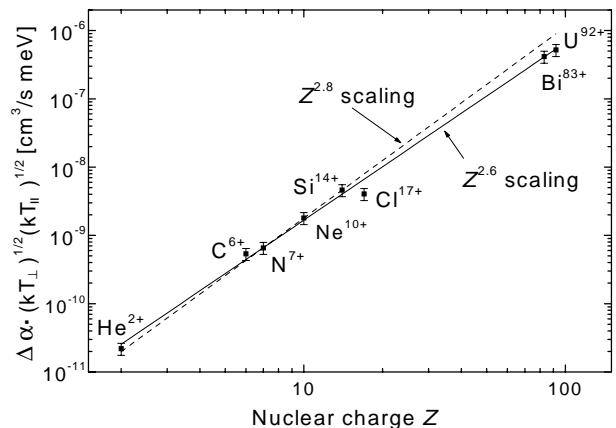


Figure 1: Dependence of the scaled excess rate $kT_{\perp}^{0.5} \cdot kT_{\parallel}^{0.5} \cdot \Delta\alpha$ at 0 eV on the nuclear charge Z . The measurements have been performed at different storage rings (TSR, CRYRING, ESR). The excess rates have not been normalized to the same magnetic field strength. The dashed line is a $Z^{2.8}$ scaling according to [3]. The full line is the new $Z^{2.6}$ scaling with inclusion of the Bi⁸³⁺ and U⁹²⁺ data.

could be observed. This decrease of ion beam quality is in accordance with previous findings at the ESR, where the transversal temperature T_{\perp} has been found to vary with magnetic field strength [2]. Hence, the oscillations in the recombination rate seem to be closely connected with changes of the ion beam properties in the transversal direction, which are introduced by small variations of the guiding field. However, the reason for this peculiar behaviour is not known yet. Apart from the oscillations an overall increase of the rate enhancement with increasing magnetic field is found.

For less heavy bare ions ($Z < 18$) a $Z^{2.8}$ scaling of the scaled excess rate $kT_{\perp}^{0.5}kT_{\parallel}^{0.5}\Delta\alpha$ has been reported [3]. When the two measurements for Bi⁸³⁺ and U⁹²⁺ are included this behaviour slightly changes to a $Z^{2.6}$ scaling.

Determination of $2s_{1/2} - 2p_{1/2}$ energy splitting of Li-like heavy-ions by means of DR

Li-like ions are the simplest ions in which $\Delta n = 0$ excitations ($2s_{1/2} \rightarrow 2p_{1/2}$ and $2s_{1/2} \rightarrow 2p_{3/2}$) are possible from the ground-state, thus providing $1s^2 2p_{1/2,3/2} n l_j$ -DR-resonances in the low-energy domain. For a comprehensive theoretical description of the measured DR features of the heavy ions under investigation (Au⁷⁶⁺, Pb⁷⁹⁺, Bi⁸⁰⁺ and U⁸⁹⁺) a fully relativistic treatment is needed. In addition, radiative (QED) corrections scale approximately with Z^4 and therefore become increasingly important. The same is true for corrections caused by the finite size of the atomic nucleus and by relativis-

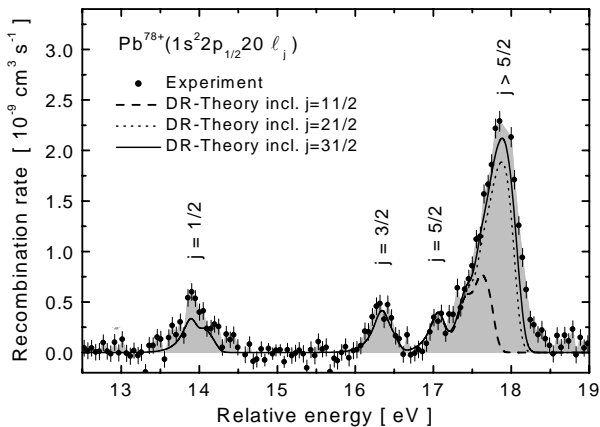


Figure 2: Measured Pb^{79+} recombination rate coefficient compared with our fully relativistic theoretical calculation (full line). The theory has been shifted by -0.65 eV (see text) .

tic effects. Up to now for DR in Li-like very heavy ions there are no strict QED calculations which allow for a direct comparison with the experiment and hence a testing of QED in strong fields. On the other hand a large number of QED calculations for the $2s - 2p$ splitting in Li-like ions are available, mainly triggered by the accurate measurements of Schweppe et al. for U^{89+} [4]. We have developed a novel method which allows to extract excitation energies of the projectile ions from the DR resonance positions of the doubly excited recombined ion. For every excitation channel of the dielectronic capture an infinite number of dielectronic resonances converging to the associated series limit may be observed. The main idea is to extrapolate the energies of individual Rydberg resonances to the associated series limit. For increasing values of n and there especially for high angular momenta j the mutual influence of core and Rydberg electrons can be neglected and the excitation energy E_∞ can be described by

$$E_\infty(Z) = E_{Res}(Z, n, j) + E_B(Z, n, j), \quad (1)$$

where $E_{Res}(Z, n, j)$ is the resonance energy and $E_B(Z, n, j)$ the binding energy of the Rydberg electron, e.g. in a H-like approximation (Dirac energies). Therewith, one deals with a multitude of resonances the energy dependence of which is well known. Beside the series limit as one fitting parameter, additional free parameters can be introduced to improve the energy calibration.

In particular, for very heavy Li-like ions all $1s^2 2p_{1/2} n \ell_j$ resonance manifolds with $n \geq 20$ can be found within the energy range (0-400 eV) which is accessible by our present experimental set-up. Individual Rydberg states up to $n \approx 45$ have been observed. For Rydberg states with $n = 20 - 25$ detailed information about the fine-structure and resonance strengths could be obtained (see Fig. 2). As can be seen from the figure a very good agreement between the experiment and fully relativistic calculation (GRASP code) is found as long as the *shapes* and the *resonance strengths* of the DR-resonances are concerned. This agreement is even more striking as the experimental rate coefficient has been measured on an absolute scale, and hence theory and experiment are not normalized with respect to each other. It should be noted that the inclusion of very high angular momentum components ($j_{max} \gtrsim 23/2$) is needed. On the other hand it is known that uncertainties in absolute energies

produced by the GRASP code are ≈ 1 eV or even more, which are mainly caused by the approximations used to include QED in the MCDHF code. But the additional theory-based knowledge about the shape and the fine-structure of the doubly excited Rydberg states can be used to improve the accuracy of the extrapolation significantly.

With the method described above the following values for the $2s_{1/2} - 2p_{1/2}$ splitting have been obtained: $E_\infty(\text{Au}^{76+}) = 216.11(20)$ eV, $E_\infty(\text{Pb}^{79+}) = 230.62(20)$ eV and $E_\infty(\text{U}^{89+}) = 280.56(20)$ eV. These results are sensitive to QED contributions of the order α^2 . A further reduction of the error by a factor of ≈ 5 can be expected in the near future as the main source of errors is the available knowledge of the velocity distribution of the cooler electrons. This distribution can be probed with high accuracy with an ion of lower nuclear charge Z . In contrast to the very heavy ions, isolated resonances with small natural linewidth (" δ -like") are expected, so that a measured spectrum reflects the velocity distribution of the target electrons. Details can be found in [5].

Scaling behaviour of DR Rydberg states

As mentioned above, one strength of DR investigations utilizing storage ring coolers is the measurement of *absolute* rate coefficients. This allowed us to determine the scaling behaviour of the resonance strength $S = \int \sigma(E) dE$ of the Rydberg series of Pb^{79+} (Fig. 3). For the doubly excited Rydberg states a $E^{-1}n^{-3}$ scaling can be expected as $S_{Res} \propto A_a \cdot \omega$, the autoionisation rate $A_a \propto n^{-3}$ and the fluorescence yield $\omega \approx const.$ for sufficiently high n . A comparison (Fig. 3) between experimental resonance strengths for the DR of Pb^{79+} , reveals a n^{-3} scaling law and DR/MCDF calculations for $n = 20 - 25$ confirm these predictions.

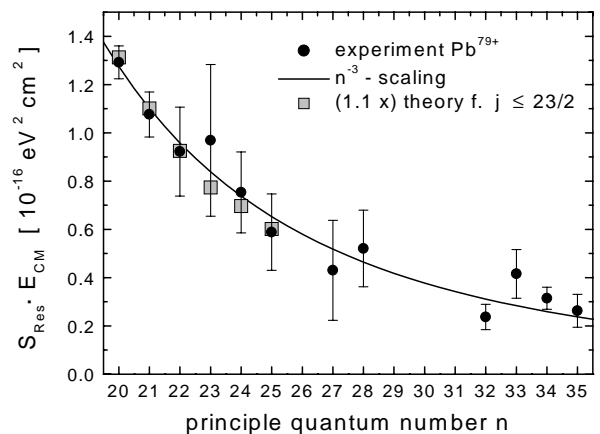


Figure 3: $E^{-1}n^{-3}$ scaling of the DR resonance strength S_{Res} of $\text{Pb}^{78+}(1s^2 2p_{1/2} n \ell_j)$ -resonances (DR of Pb^{79+}). The full circles are experimental data, the full line is a scaling according to $E \cdot S_n = E \cdot S_{n=20} \cdot 20^3/n^3$. The grey squares are DR/MCDF calculations (GRASP). Theory has been multiplied by a factor 1.1 in order to take states into account with $j > 23/2$.

References

- [1] M. Steck, GSI Workshop, June 21, 1997.
- [2] A. Hoffknecht et al., PRA **63**, 012702 (2000) and: A. Hoffknecht et al., GSI Sci. Rep. 1999, p. 88.
- [3] H. Gao et al., JPB **30**, L499 (1997).
- [4] J. Schweppe et al., PRL **66**, 1434 (1991).
- [5] C. Brandau, Dissertation (Uni Giessen), <http://bibd.uni-giessen.de/ghtm/2001/uni/d01008.htm>

Fragmentation of Atoms in Strong Fields viewed with Reaction-Microscopes

R. Moshhammer^{1,2}, H. Kollmus^{1,2}, S. Hagmann^{2,3,4}, M. Schulz⁵, B. Feuerstein², R. Mann³, A. Dorn², D. Fischer², A. N. Perumal², C. Höhr², C.D. Schröter^{1,2}, J.R. Crespo Lopez-Urrutia², H. Rottke⁶, C.Trump⁶, W. Sandner⁶, R.E. Olson⁵, J. Ullrich^{1,2}

¹MPI-Heidelberg, ²Uni Freiburg, ³GSI Darmstadt, ⁴KSU Manhattan, ⁵UMR Missouri, ⁶MBI Berlin

The interaction of both, highly charged ions and intense lasers fields, with matter or atoms attract increasing interest because of fundamental questions to be addressed and because of the long term perspectives of potential applications. Such applications cover a wide range from inertial fusion driven by heavy ion or intense laser beams to new techniques in material science and medical treatments. These developments rely on a profound knowledge about the interaction of radiation with single atoms and about the dynamical correlation of electrons in ultra-short and strong fields. In this context ionization of atoms in intense fields plays a key role because the coupling between radiation and matter is mediated by the electrons.

Theoretically, in particular the regime of large perturbations is of interest, where the radiation field strongly modifies the atomic states, where it interacts simultaneously with several electrons and where non-linear effects prevail. This puts severe constraints on theoretical descriptions revealing substantial problems in the treatment of the correlated motion of mutually interacting particles under the action of a time dependent force. In spite of these difficulties, successful theoretical approaches have been developed so far for single ionization of atoms by charged heavy-ion impact as well as by intense laser pulses. But, the extension to more complicated situations like e.g. double or multiple ionization has been identified as a key challenge for many-body Coulomb theories.

Experimentally, the recent developments of advanced many-particle coincidence techniques to study atomic fragmentation allow to identify simultaneously the momenta of all reaction products emerging from a single collision with high resolution. These so called reaction microscopes consist of recoil-ion momentum spectrometers combined with an electron analyzer with 4π efficiency and high momentum resolution. They enable experiments on single and multiple ionization reactions of atoms and molecules with unprecedented completeness and momentum resolution (for a review see [1]). Such kinematically complete experiments provide benchmark data for theories and allow for the first time the separation of different mechanisms involved in the ionization process.

In this report we discuss three topics concerning the fragmentation of atoms in the strong fields generated by fast passing highly-charged ions and intense low-frequency laser pulses. The experiments have been performed at the UNILAC of GSI and at the high power laser facility of the Max-Born-Institute in Berlin.

Ultimate Tests of Single Ionization Theories at Strong Perturbations

In a kinematically complete experiment the emission of low energy electrons ($E_e < 150$ eV) in single ionization of He-atoms induced by 3.6 MeV/u Au^{53+} ion impact has been studied. Using a reaction-microscope [1] the momenta of the recoiling target-ions and of the ejected electrons have been measured in

coincidence. In a previous work the electron energy and angular distribution was studied irrespective of the projectile scattering [2]. These double differential electron emission cross sections have been shown to be in very good agreement with continuum distorted wave eikonal initial state (CDW-EIS) calculations. Because of the large perturbation of the projectile ion with $q/v = 4.4$ (the projectile charge to velocity ratio in atomic units is a measure of the perturbation strength. Perturbation theory usually can be applied for $q/v < 1$.), a strong postcollision effect has been observed even at very low electron energies. The receding projectile drags the electrons into the forward direction. As a next step in testing theory in more detail, we investigated the electron emission characteristics as a function of the momentum transferred from the projectile to the target atom. In almost all cases the longitudinal momentum transfer (i.e. the component along the beam direction) is very small compared to the transverse direction. This quantity is deduced from the measured vector momenta of the electron and the recoiling target ion using momentum conservation. In this way projectile scattering angles as small as 20 nrad became accessible, enabling for the complete determination of the three particle dynamics in singly ionizing heavy-ion atom collisions.

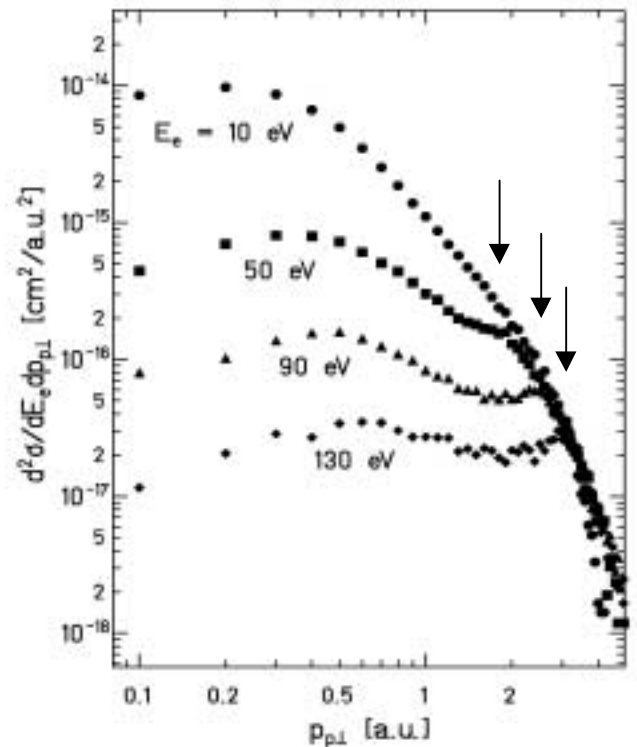


Figure 1: The projectile momentum transfer in the transverse direction for given electron energies in single ionization of He by 3.6 MeV/u Au^{53+} impact. A transverse momentum transfer of $p_{\perp} = 1$ a.u. corresponds to a scattering angle of 250 nrad.

In fig. 1 the distribution of the transverse momentum transfer is shown for fixed ejected electron energies. Low energy electron emission is dominated by small transverse momentum transfers indicating that mainly dipole-transitions from the initially bound to the continuum state contribute [3]. In this so called soft collision regime the fast passing projectile acts much like a source of virtual photons which get absorbed by the target atom revealing similarities with photoionization [4]. With increasing electron energy more violent encounters contribute. Then, the momentum transfer exhibits a peak at a value which is equal to the momentum of the ejected electron (arrows in fig. 1) clearly demonstrating the transition to the binary-encounter regime: the target electron is knocked out in a binary collision with the projectile.

In addition, triple differential cross sections (TDCS) for these highly non-perturbative collisions have been measured. There the angular distribution of the ejected electron in the plane defined by the incoming and the scattered projectile (i.e. in coplanar geometry) is plotted for a given electron energy and for fixed momentum transfer. Such TDCS data are known to be very sensitive on the collision dynamics and they can be considered as the ultimate test of single ionization theories in the non-perturbative regime.

Electron-Electron Interaction in Projectile Ionization: A New Way to Explore (e,2e) on Ions ?

Measurements of differential cross sections for ionization of ions in collisions with high-energy electrons are extremely difficult to perform by applying conventional crossed beams techniques. In essence, due to the low luminosity, such experiments have not been possible up to now, not even in storage rings. If feasible, they would allow for instance high precision momentum spectroscopy of bound states in few-electron heavy-ions.

On the other hand, in a fast collision of a non-bare projectile-ion with a target atom the projectile can be ionized via an interaction with one of the target electrons (electron-electron (e-e) interaction). In those collisions both, the active target electron and the projectile electron, get ionized [5]. This process is equivalent to electron impact ionization of the projectile if the initially bound target electron can be treated as a quasi free electron. In such a scenario, using a dense atomic beam, one would circumvent the above mentioned low luminosity problem of conventional crossed beams experiments. But, there is a second mechanism contributing to projectile ionization: Interaction of the electron with the target nucleus (nucleus-electron (n-e) interaction). Thus, electron impact ionization of ions may be studied in very detail, if the many-particle dynamics is completely controlled experimentally.

Such a measurement has been performed at the UNILAC of GSI studying ionization of 3.6 MeV/u C^{2+} projectiles in collisions with He atoms. In the experiment the final state momentum vectors of all particles emerging from the collision have been mapped. In the following we will demonstrate that a separation of the two competing mechanisms contributing to projectile ionization is indeed possible, because different mechanisms populate kinematically different regions in the final state. If a (n-e) interaction takes place the target nucleus

has to deliver the momentum transfer required to ionize the projectile. Thus, one expects a recoiling He^{1+} target ion with large momentum, whereas the target electron acts as a spectator. In contrast, in a (e-e) interaction the target electron plays the active role and the He-nucleus takes part as a spectator [6]. Therefore the two processes ((n-e) and (e-e)) can be separated event by event by putting a condition on the values of the momenta of the target electron p_{ele} and the He^{1+} ion p_{ion} . Selecting only those events, for which $p_{ele} > p_{ion}$ is fulfilled, implies that mainly the (e-e) interaction is left in the resulting subset of the experimental data. The validity of this approach is demonstrated in the fig. 2. There, the momentum distributions of the projectile electron, the target electron and the He^{1+} recoil-ion are projected onto the collision plane. This plane is defined by the incoming projectile momentum and the momentum transfer. As expected for (e-e) interaction, the ionized projectile electrons and the target electrons are preferentially emitted into opposite directions. The target ion behaves as a spectator and therefore exhibits no angular correlation with the emitted electrons.

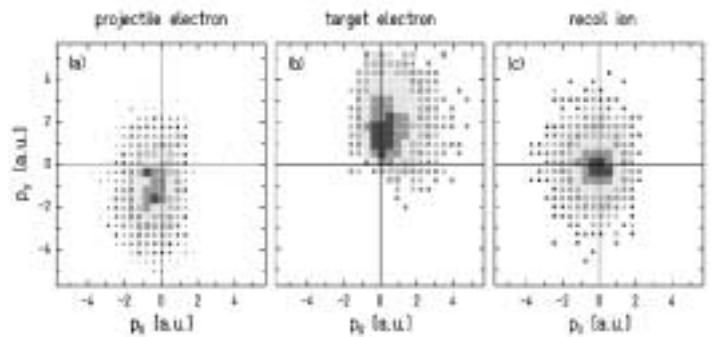


Figure 2: The momentum distributions of the projectile electron (in the projectile frame), the target electron and the He^{1+} recoil-ion projected onto the collision plane.

The experimental data are in very good agreement with classical trajectory Monte-Carlo (CTMC) calculations. According to these theoretical results more asymmetric collision partners with respect to the binding energies of the active electrons are required to fulfill the equivalence to electron impact ionization. Such experiments are in preparation and will be performed in near future in the storage ring ESR at GSI using one-electron heavy-ions and light or even excited targets as a dense electron target. Then, as a long term perspective, fully differential cross sections for electron impact ionization of few-electron heavy-ions will become accessible.

Double Ionization of Neon by Intense Laser Pulses

It is almost 20 years ago, that unexpected large yields for the creation of doubly charged ions were observed when atoms are exposed to intense laser fields [7]. This enhancement, termed non-sequential ionization, which can amount to several orders of magnitude, is a consequence of the electron-electron correlation, but the underlying mechanism remained unclear over many years (for a review see [8]). Among many others a classical rescattering model was proposed by Corkum [9] to explain double ionization. In this model the first ionized

electron is driven by the electric field of the laser pulse and thrown back to its parent ion knocking out a second electron in an (e,2e)-like collision. Many experimental findings, and in particular recent ion momentum measurements [10,11], favor the rescattering model. But, to ultimately unravel the many-particle dynamics of double ionization in intense laser fields a complete determination of the final state is required, i.e. the determination of the momentum vectors of all atomic fragments. Up to now, such a measurement was beyond experimental capabilities.

We succeeded in performing a first kinematically complete experiment on double ionization of Ne by ultra-short (25 fs) laser pulses ($\lambda = 800$ nm) at an intensity of 10^{15} W/cm². The created ion and up to two electrons were detected in coincidence using a reaction microscope. In the experiment the momentum vectors of all three particles (electrons and ion) and the charge state of the ion were determined.

energy, which can be as large as $2U_p$ (U_p is the mean quiver energy), maximizes if the electron is born at a time when the electric field goes through zero. In the rescattering model for double ionization the (e,2e)-like collision with the returning electron occurs very close to such a zero crossing. Hence, electron energies up to $2U_p$ are expected in agreement with our experimental finding. Even though the electron motion is dominated by the ponderomotive force the signature of the (e,2e) collision dynamics is still preserved in the final state. In particular the analysis of correlated two electron spectra, which are not discussed here, yield more detailed information about the fragmentation in strong laser fields.

For the future, experimental studies of electron correlation in strong laser fields will be feasible using a large variety of targets, like e.g. atoms, clusters and molecules. On this road in particular a kinematically complete experiment on helium, the most simple two electron system, remains as an experimental challenge.

This work was supported by the Gesellschaft für Schwerionenforschung, the Max-Born-Institute, the Leibniz-program and the SFB 276 project B8 of the Deutsche Forschungsgemeinschaft DFG, and BMBF.

References

- [1] R. Dörner et al., Phys. Rep. 330, 95 (2000)
- [2] R. Moshhammer et al., Phys. Rev. Lett. 83, 4721 (1999)
- [3] M. Inokuti, Rev. Mod. Phys. 43, 297 (1971)
- [4] R. Moshhammer et al., Phys. Rev. Lett. 79, 3621 (1997)
- [5] E.C. Montenegro et al., Adv. At. Mol. Opt. Phys. 34, 249 (1994)
- [6] R. Dörner et al., Phys. Rev. Lett. 72, 3166 (1994)
- [7] A. L'Huillier et al., Phys. Rev A 27, 2503 (1983)
- [8] M. Protopapas et al., Rep. Prog. Phys. 60, 389 (1997)
- [9] P. Corkum, Phys. Rev. Lett. 71, 1994 (1993)
- [10] Th. Weber et al., Phys. Rev. Lett. 84, 443 (2000)
- [11] R. Moshhammer et al., Phys. Rev. Lett. 84, 447 (2000)

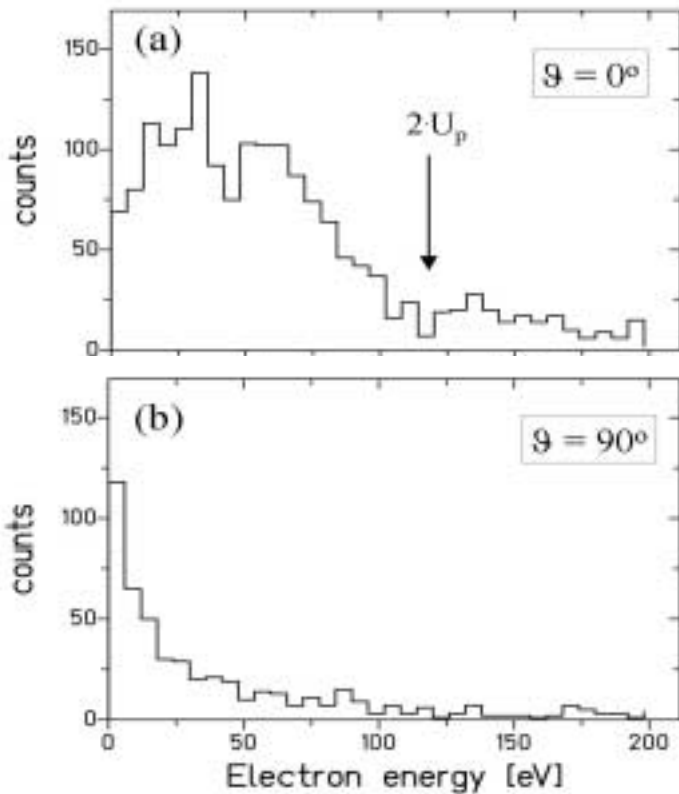


Figure 3: The electron energy distributions for emission along ($\vartheta = 0^\circ$) and perpendicular ($\vartheta = 90^\circ$) to the light polarization axis in double ionization of Ne by 10^{15} W/cm² laser pulses.

In contrast to single ionization, which is dominated by the emission of low energy electrons ($E_e < 20$ eV), for double ionization high energetic electrons with energies of more than 120 eV have been observed (fig. 3). In both cases electrons are preferentially emitted along the light polarization axis (i.e. along the electric field direction of the laser field). In fact, after being released from the atom the electrons perform a quiver motion in the external laser field. They are driven by the ponderomotive force mediated by the electric field in the light pulse. The final kinetic drift energy of the ionized electron after the end of the laser pulse depends on the phase of the oscillating electric field at which the electron was set free. This

Three body fragmentation of CO₂ in collisions with 5.9 MeV/u Xe¹⁸⁺ and Xe⁴³⁺ ions

B. Siegmann, I. Küster, U. Brinkmann, U. Werner, H.O. Lutz, University of Bielefeld
R. Mann, GSI Darmstadt

The multiple ionization and fragmentation of CO₂ by fast Xe¹⁸⁺ and Xe⁴³⁺ ions was studied utilizing a position- and time-sensitive multi-particle detector which allows the coincident measurement of the momenta of correlated fragment ions. The experiment has been performed using the highly charged ion beam of the UNILAC at the GSI Darmstadt. The slow fragment ions and electrons generated in the collision process are separated by a weak electric field. Electrons were detected by a channeltron at one side of the interaction region; positive ions were accelerated towards the time- and position-sensitive multi-particle detector at the other side [1,2]. For each positive fragment ion the position and the time-of-flight relative to the electron signal were recorded. Of special interest are the Coulomb explosion processes where all fragments are positively charged. For these reaction channels the coincident measurement of the momenta of correlated fragment ions yields a kinematically complete image of the molecular break-up process, and the kinetic energy release as well as angular correlations can be derived for each individual event. In collisions of fast highly charged Xe-ions with CO₂ coincidences with a total charge of at least 6 are clearly separated. Among the various observed reaction channels the reactions C^{q+} + O^{p+} + O^{r+} fulfill the conditions for a kinematically complete description of the fragmentation process. For these reactions the fragmentation dynamics may be analyzed in terms of three independent parameters. A practical choice of the characteristic variables consists of the kinetic energy release and the angles χ and θ_v in velocity space [3].

Fig. 1 shows the kinetic energy release spectrum and the measured distribution of the angles χ and θ_v observed in C⁺+O⁺+O⁺ fragmentation in collisions with 5.9MeV/u Xe¹⁸⁺ and Xe⁴³⁺. All three characteristic parameters are independent of the projectile charge measured here. The maximum of the measured kinetic energy distribution is in good agreement with the prediction of the point charge Coulomb explosion model.

The angle χ , defined by the relative velocity of the O⁺-ions \vec{v}_{OO} and \vec{v}_C , is an indicator whether the molecular bonds break simultaneously or in a stepwise fashion [4]. The χ distribution shows a peak around 90 degrees which is consistent with a simultaneous break up of the molecular bonds. A break-up of the molecular bonds in a time short on a time scale defined by rotational and vibrational periods of the system leads to a strong angular correlation between the corresponding velocities which shows up as a narrow peak in the χ -distribution. In case of a two-step process the correlation would be lost resulting in a uniform χ -distribution.

The angle θ_v , defined by the two relative \vec{v}_{CO} velocities, is closely connected with the O-C-O bond angle. For Carbon-dioxide as a linear molecule the maximum of the O-C-O bond angle would be expected around 180

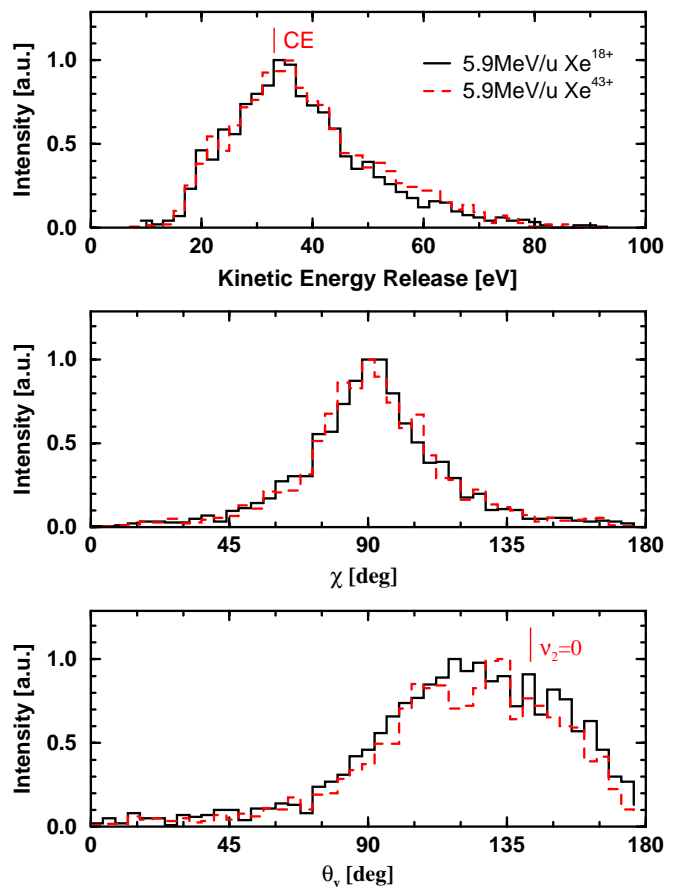


Figure 1: Kinetic energy release and angles χ and θ_v derived from coincident C⁺+O⁺+O⁺ fragments in collisions with 5.9 MeV/u Xe^{q+}. The energy release predicted by the Coulomb explosion model (CE) and the most probable angle θ_v expected for the bending mode $\nu_2 = 0$ are marked in the figure.

degrees. The θ_v -distribution observed in collisions with fast highly charged ions is clearly shifted to smaller angles with a broad maximum around 120 degrees. This can be qualitatively understood taking into account the vibration modes of CO₂. Using a harmonic oscillator potential to describe the bending-mode groundstate ($\nu_2 = 0$) leads to a most probable “bond angle” of $\beta \approx 172.5$ degree. In the Coulomb explosion model this angle corresponds to an angle $\theta_v \approx 142^\circ$ in velocity space which is in good qualitative agreement with the experimental results.

References

- [1] J. Becker et al., Nucl. Instrum. Methods **A337**, 409 (1994)
- [2] U. Werner et al., Nucl. Instrum. Methods **B124**, 298 (1997)
- [3] B. Siegmann et al., Aust. J. Phys. **52**, 545 (1999)
- [4] U. Werner et al., Phys. Rev. Lett. **74**, 1962 (1995)

Experiments with Heavy Ions in Traps

Caen¹, CERN², GSI³, Jyväskylä⁴, Leuven⁵, Mainz⁶, Michigan⁷, Montreal⁸, München⁹, Orsay¹⁰
and the SHIPTRAP Collaboration

HITRAP: A Facility for Experiments with Trapped Highly Charged Ions

W. Quint³, J. Dilling³, S. Djekic⁶, H. Häfner³, H.-J. Kluge³, G. Marx³, D. Rodríguez³, J. Schönfelder³, G. Sikler³, T. Valenzuela⁶, J. Verdú³, C. Weber³ and G. Werth⁶

The GSI midterm project HITRAP is a planned ion trap facility for capturing and cooling of highly charged ions (HCI) produced at GSI in the heavy-ion complex of the UNILAC-SIS accelerators and the ESR storage ring. In this facility heavy highly-charged ions up to uranium will be available as bare nuclei, hydrogen-like ions or few-electron systems at low temperatures. The trap for receiving and studying these ions is designed for operation at extremely high vacuum by cooling to cryogenic temperatures. The stored highly charged ions can be investigated in the trap itself or can be extracted from the trap at energies up to about 30 keV/q.

The basic components constituting the HITRAP facility are outlined in Fig. 1. Highly charged ions are accelerated in the heavy-ion synchrotron SIS, stripped in a foil to the desired charge state and injected into the Experimental Storage Ring (ESR). For bare or hydrogen-like ions, energies of a few hundred MeV/u are required. In the ESR the ions will be decelerated to an energy of 3 MeV/u. It is planned to demonstrate this low-energy operation mode of the ESR during 2001. They will then be extracted in a fast-extraction mode as short ion bunches.

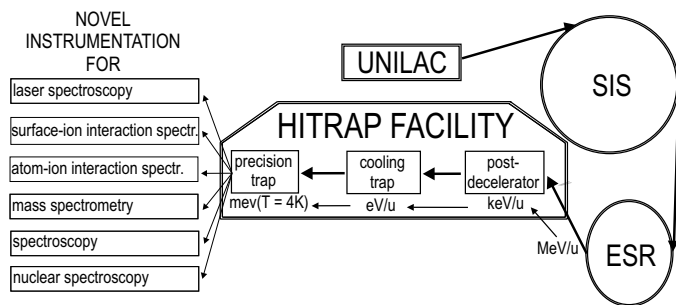


Figure 1: Schematic of the GSI accelerator complex and the planned HITRAP facility. Highly charged ions are extracted from the ESR storage ring at 3 MeV/u, decelerated in a post-decelerator to some keV/u, and then transferred into a Penning trap system.

The extracted ion bunches will be post-decelerated to a final energy of the order of 30 keV/q in a radiofrequency quadrupole structure (RFQ) or a linear interdigital H-mode (IH) drift tube structure. Recently, a RFQ decelerator has been successfully commissioned at the Antiproton Decelerator (AD) at CERN to allow antiprotons to be decelerated from an energy of 5.3 MeV down to below 100 keV. After post-deceleration the ions will be cap-

tured into a first Penning trap (Fig. 1) and cooled to a temperature of $T = 4$ K with a combination of electron or positron cooling and resistive cooling. The cooled highly charged ions can be extracted and transferred to physics experiments. The HITRAP facility will provide about 10^6 charges per second, i.e. about 10^4 ions/s in the case of U^{92+} .

The HITRAP physics programme includes collision studies with highly charged ions at well-defined low energies (eV/u), laser spectroscopy of hyperfine structure transitions in HCI, X-ray spectroscopy on HCI, and high-accuracy measurements to determine the magnetic moment anomaly (or *g-factor*) of the electron bound in hydrogen-like heavy ions and the atomic binding energies of few-electron systems.

For the determination of the *g-factor* of the bound electron in highly charged ions as a stringent test of Quantum Electrodynamics (QED) [1] a precision Penning trap has been developed in a joint effort of the University of Mainz and GSI. The *g-factor* of the bound electron is determined from the Larmor precession frequency ω_L of its magnetic moment in the magnetic field B , $\omega_L = g(e/2m_e)B$, and the cyclotron frequency of the hydrogen-like ion, $\omega_c = (Q/M)B$.

$$g = 2 \cdot \frac{\omega_L}{\omega_c} \cdot \frac{Q/M}{e/m_e}. \quad (1)$$

Our measurement of the *g-factor* of the electron in hydrogen-like carbon ($^{12}\text{C}^{5+}$) yielded a value of $g_e^{exp}(\text{C}^{5+}) = 2.001\,041\,596(5)$, in excellent agreement with the theoretical value of $g_e^{th}(\text{C}^{5+}) = 2.001\,041\,591(7)$ [2]. Further improvement of the theoretical [3] as well as the experimental accuracy will make it possible to determine the atomic mass of the electron with an unprecedented precision of a few parts in 10^{-10} . In 2000 we performed a *g-factor* measurement on hydrogen-like oxygen ($^{16}\text{O}^{7+}$). The preliminary experimental value of $g_e^{exp}(\text{O}^{7+}) = 2.000047017(8)$ is in excellent agreement with the theoretical prediction of $g_e^{th}(\text{O}^{7+}) = 2.000\,047\,022(5)$. This is our second high-accuracy test of bound-state QED. At the HITRAP facility, the *g-factor* measurements will be performed up to the heaviest hydrogen-like ions, where the product of proton number and fine-structure constant ($Z\alpha$) approaches unity. This will provide a crucial test of QED calculations in extreme electromagnetic fields.

High Accuracy Mass Determination of unstable Nuclei with the Penning Trap Mass Spectrometer ISOLTRAP

F. Ames², G. Audi¹⁰, D. Beck³, K. Blaum³, G. Bollen⁷, J. Dilling³, O. Engels⁹, F. Herfurth^{3,9}, A. Kellerbauer², H.-J. Kluge³, D. Lunney¹⁰, R.B. Moore⁸, M. Oinonen², C. Scheidenberger³, S. Schwarz⁵, G. Sikler³, E. Sauvan², J. Szerypo⁴ and C. Weber³

The Penning trap mass spectrometer ISOLTRAP is installed at ISOLDE/CERN. It provides mass measurements of short-lived nuclides with very high accuracy. Accurate experimental mass values serve for testing nuclear models, help to increase their predictive power for nuclides far from stability and can reveal nuclear structure. Additionally, some mass values represent important input parameters for Standard Model tests and astrophysical calculations.

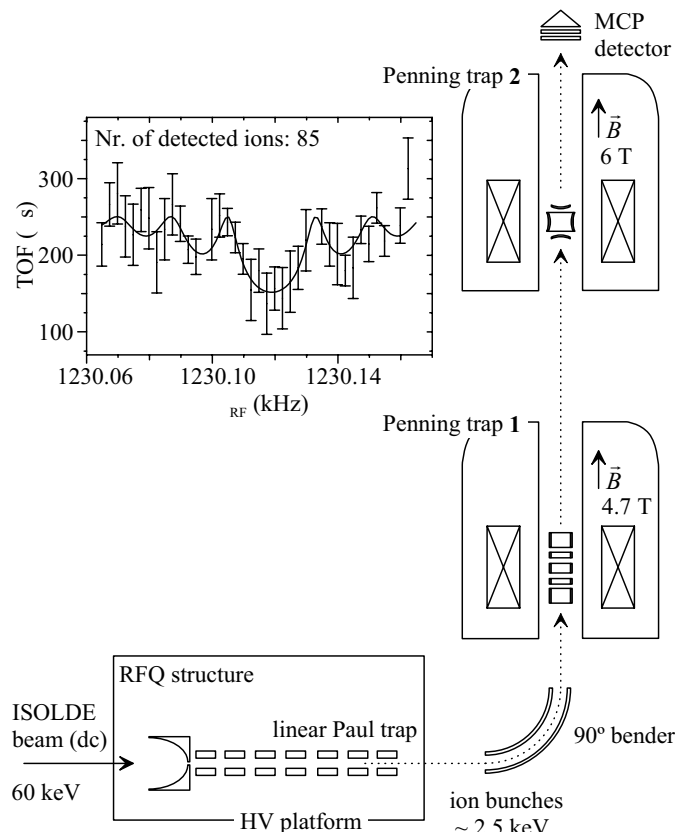


Figure 2: Experimental setup of the ISOLTRAP spectrometer. The inset shows the cyclotron resonance curve for ^{74}Rb . Plotted is the time of flight (TOF) of the ions from the trap to the ion detector as a function of the applied radiofrequency with the theoretical line shape fitted. This spectrum contains roughly one fourth of all ^{74}Rb data obtained during a recent run.

The ISOLTRAP Penning trap mass spectrometer (Fig. 2) consists of three main parts: a) a linear gas-filled radiofrequency quadrupole (RFQ) trap for retardation, accumulation, cooling and bunched ejection at low energy [4], b) a gas-filled cylindrical Penning trap for further cooling and isobaric separation [5], and c) an ultra-high vacuum hyperbolic Penning trap for isomeric separation and the mass measurement [6]. The mass measurement is performed via the determination of the cyclotron frequency $\omega_c = q/m \cdot B$ of the ion with mass m and charge q revolving in the magnetic field of strength B . The accuracy of the measured mass values is typically $\delta m/m = 1 \cdot 10^{-7}$.

Six radioactive beam times were carried out in 2000. In the first beam time, an uranium carbide target was used in conjunction with the resonant ionisation laser ion source (RILIS) to measure the mass of neutron-rich tin isotopes.

The isotopes $^{128,129,130,132}\text{Sn}$ were investigated. Particularly, the mass of the doubly magic ^{132}Sn is of interest for astrophysical calculations along the r-process path.

The second beam time was dedicated to neutron-deficient Sr isotopes. The mass of ^{76}Sr and ^{77}Sr could be measured by determining the mass of SrF_2 molecules. ^{76}Sr is a possible waiting point on the astrophysical rp-process path.

One major project in 2000 was the measurement of the Q -value of the superallowed β -decay of ^{74}Rb . Two beam times were performed to measure the mass of ^{74}Rb (Fig. 2) and its daughter nucleus ^{74}Kr . ^{74}Rb is the shortest-lived nuclide ever investigated in a Penning trap ($T_{1/2} = 65$ ms). The accuracy of its mass value is governed by statistics and resolving power, which are limited by production rate and half-life. The relative accuracy reached for the mass of ^{74}Rb is about $3.4 \cdot 10^{-7}$ (i.e. ≈ 25 keV). The measurement of ^{74}Kr was performed with an unprecedented relative accuracy of only $3 \cdot 10^{-8}$. Additionally, the masses of the krypton isotopes with $A = 73$ and 75 were measured.

One beam time was performed using a molten lead target to complete the picture of binding energies for the neutron-deficient mercury isotopes. The isotopes $^{179,180,181}\text{Hg}$ were measured for the first time closing the gap in the binding energy systematics.

The last beam time in 2000 was used to measure the mass of ^{34}Ar produced in a CaO target. This value is needed with very high accuracy in the context of the FT-value systematics for superallowed Fermi β decays. ISOLTRAP succeeded in measuring this mass with an uncertainty below 1 keV.

Future mass measurements will be performed in astrophysically interesting regions like the neutron-rich Cd and Sn isotopes, the neutron-deficient Y isotopes and around the rp-process waiting points ^{68}Se and ^{72}Kr . Additionally, the measurements in the context of fundamental tests will be continued measuring ^{32}Ar . Future technical developments focus on the improvement of the overall efficiency by improving the detector setup as well as different parts of the ion transfer.

Status of the SHIPTRAP project: A capture and storage facility for heavy radionuclides from SHIP

G. Marx³, D. Ackermann³, J. Dilling³, F.P. Heßberger³, S. Hoffmann³, H.-J. Kluge³, R. Mann³, G. Münzenberg³, Z. Qamhieh³, W. Quint³, D. Rodríguez³, M. Schädel³, J. Schönfelder³, G. Sikler³, C. Toader³ and C. Weber³

The ion trap facility SHIPTRAP is being set up to deliver very clean and cool beams of singly-charged recoil ions produced at SHIP at GSI [7]. SHIPTRAP consists of a gas cell for stopping and thermalizing high-energy recoil ions from SHIP, an rf ion guide for extraction of the ions from the gas cell, a linear rf trap for accumulation and bunching of the ions, and a Penning trap for isobaric purification. The recent development for the SHIPTRAP stopping chamber and the extraction system is described in a separate section later in this report.

The Buncher

The ion bunching system is a 1 m long Radio Frequency Quadrupole (RFQ) immersed in a low-pressure buffer gas. The four rods have a diameter of 9 mm at a distance between two opposite rods of 7.86 mm. The rods are divided into 34 segments. With proper choice of applied voltages, one creates a potential slope with a harmonic potential well at the end of the quadrupole structure. When the ions lose energy in collisions with the buffer gas, they accumulate in this trap and can be extracted as a short bunch of cool ions. The radial motion in the RFQ is described by the Mathieu equations, where the solutions are characterized by the two dimensionless parameters a and q , but only $q = \frac{2eV_{rf}}{m\omega_{rf}^2 r_0^2}$ depends on the rf-amplitude. Presently we use the RFQ in a rf-only mode with no additional bias ($a = 0$). The ion motion is stable only in a certain range of q , for other values the amplitudes of the motion grow infinitely. For a certain rf amplitude V all ions of different masses whose q is below the stability limit of $q = 0.908$ pass through the buncher.

In first tests (no axial trapping) in the rf-only mode with a calibrated ion source a transmission of about 95% was achieved. Figure 3 shows a transmission plot for Ar^+ ions. The driving field frequency was set to $\nu_{rf} = 600$ kHz.

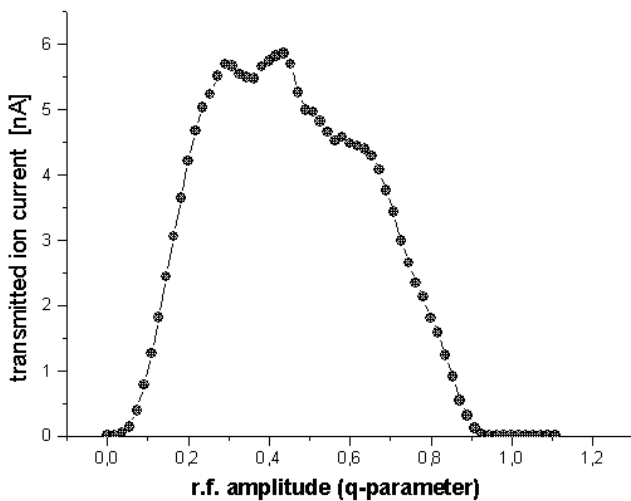


Figure 3: Transmission plot in rf-only mode for Ar^+ ions.

The basic task of the buncher at SHIPTRAP is to cool the ions from the stopping chamber and to collect them. Since the buncher will therefore be operated under buffer gas it is necessary to investigate the influence of gas on the ion motion. The average effect of ion collisions with buffer gas molecules can be approximated by a frictional drag force. This leads to the usual form of the Mathieu equation but with an added velocity dependent term. Figure 4 shows three measured transmission curves at different pressures. One can see a tendency that the right edge of the stability diagram is shifted to higher q -values. Due to the damping of the ion motion one can apply higher quadrupole field strength until the ion motion becomes unstable. The information how much the stability region is increased under buffer gas operation is important since one tries to use the limited mass resolution of the RFQ

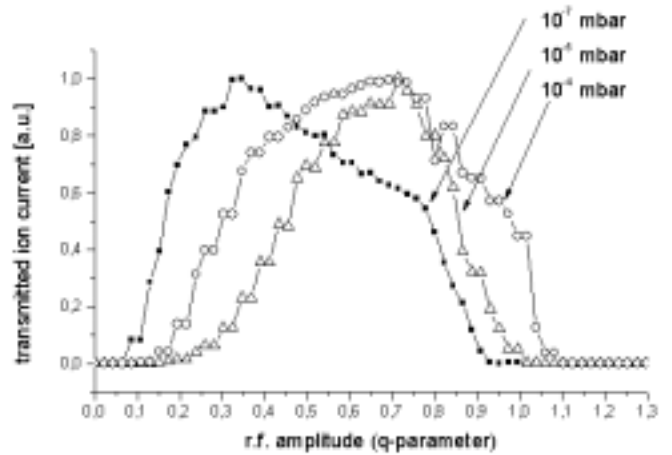


Figure 4: Influence of buffer gas on the transmission curve

in rf-only mode to suppress contamination of lighter ion species.

The Penning Trap System

Two Penning traps will be installed at SHIPTRAP, which are both housed in one superconducting magnet. The first Penning trap, a 207.5 mm long cylindrical trap with 32 mm open diameter, captures the ions from the buncher, cools and isobarically purifies them. The design is based on the one used for this purpose at the ISOLTRAP facility at ISOLDE [6]. In such a system the contaminating isotopes are very effectively suppressed due to the high mass resolving power of the cooling process. The second Penning trap, also cylindrical but shorter and with higher homogeneity in the electric and magnetic fields, will serve for precision mass measurements. The traps have been constructed, built and assembled in 2000. They are now ready for the first tests.

Summary

After an intense simulation and construction phase all components are set up and under test. SHIPTRAP will start operation in autumn 2001. The experimental programme which is envisaged by the SHIPTRAP user community promises to give new insights into the nuclear, atomic and chemical properties of the elements heavier than einsteinium.

The gas cell and extraction RFQ for SHIPTRAP

L. Beck⁹, O. Engels⁹, D. Habs⁹, J. Neumayr⁹, V. Varentsov⁹, F. Voit⁹ and A. Wilfart⁹

Set-up

The prototype of the gas cell for SHIPTRAP follows the concept of extracting the ions via the gas flow and guiding electrostatic fields. These two mechanisms can be simulated separately in first order due to the special feature of a high transmission grid in front of the nozzle. This grid prevents a loss of ions in the defocusing field inside the nozzle and improves the focusing inside the cell due to a spherical shape. The extraction RFQ separates the ions from the neutral gas. The prototype gas cell has a length and a diameter of 100 mm. The guiding field inside the

cell is created by three electrodes and a spherical grid covering the supersonic nozzle with an inner diameter of 0.6 mm. The subsonic part of the nozzle has a conical shape to achieve gas velocities high enough to drag the ions through the nozzle [8].

The design of the extraction RFQ and the electronics profits from the work done at ISOLTRAP and GSI in the past three years [4]. Compared to the structures used there the extraction RFQ of SHIPTRAP is a short structure with 12 segments and a total length of 120 mm. The diameter of the rods is 11 mm with an aperture (diameter) of 10 mm. The ions are mass selective detected in a QMS followed by a MSP (Micro Sphere Plate) [9]. The test set-up is shown schematically in Fig. 5.

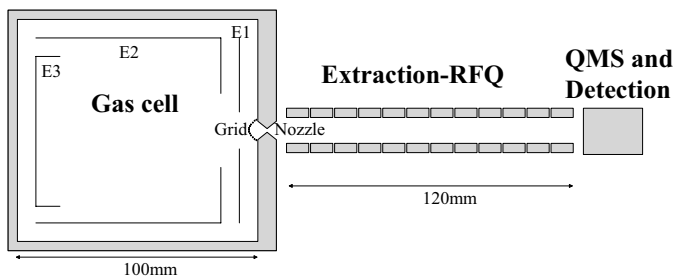


Figure 5: Test set-up for the SHIPTRAP gas cell. It consists of three electrodes (E1, E2, E3) and a nozzle covered by a high transmission grid, the extraction RFQ as a differential pumping section and the QMS and Detection section for a mass selective ion detection.

Simulations

The simulations covered the following topics: stopping of the ions in the gas (SRIM); drag of the ions via the electrical field in the cell towards a supersonic nozzle (SIMION); drag of the ions through the nozzle via the gas flow (VARJET), solving the full system of time dependent Navier-Stokes equations [10].

First stopping simulations indicate that, whatever gas is used, a majority (50 to 90%) of most radionuclides of interest could be stopped within a spheroid of 40 mm diameter and 70 mm length (for ^{232}Th at 100 keV/u in He at 50 mbar). To these values one has to add the horizontal and vertical SHIP-beam dimensions of 50 mm and 30 mm. These simulations imply the minimum dimensions for the innermost electrode of the final gas cell for SHIPTRAP.

Measurements

First measurements with laser ionized Ni and Er in the gas cell were performed to optimize the voltages in the cell and the RFQ. Based on this the extraction times in dependence of the gas pressure and the voltage inside the cell were studied. A voltage difference of 10 V was applied between the first and last segment of the extraction RFQ together with an rf-voltage of $200V_{pp}$ at 1.2 MHz to guide the ions to the mass selective ion detection system. Figure 6 shows the measured time of flight (TOF) of Ni and Er ions at different pressures and voltages in the cell.

Furthermore, the measurements showed a clear dependence of the ion focusing towards the nozzle and the grid in front of the nozzle. The grid allows to achieve faster extraction times due to higher voltages applicable in the

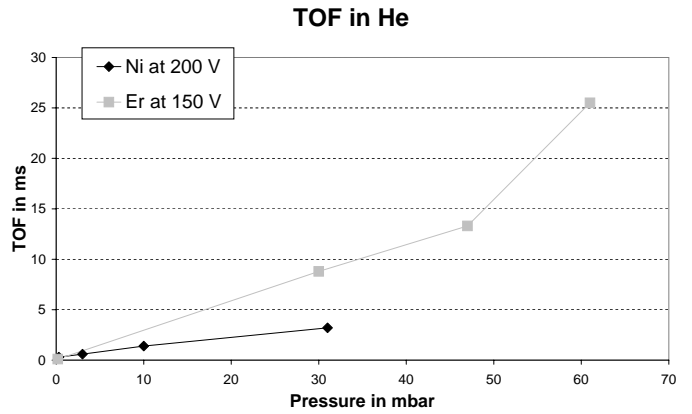


Figure 6: Measurement of the TOF of Ni and Er ions in dependence of gas pressure and voltage inside the cell (electrode E2).

cell. These higher voltages lead to a stronger defocusing of the ions. However, this drawback can be compensated by the better focusing properties of the grid.

An improved gas cell, based on these experiences is under construction. The new cell will allow higher voltages in the cell and is designed to stop and extract 90% of the ion cloud.

Optical Spectroscopy and Ion Chemistry of Trans-Fermium Elements at SHIPTRAP

H. Backe⁶, A. Dretzke⁶, G. Kube⁶, W. Lauth⁶, W. Ludolphs⁶, A. Morbach⁶ and M. Sewtz⁶

An ultra-sensitive laser spectroscopic method is being developed for the investigation of the completely unknown atomic structure of the elements No and Lr. First experiments will be performed on No which will be produced via the reaction $^{208}\text{Pb}(^{48}\text{Ca}, 2n)^{254}\text{No}$. The reaction products, separated by SHIP, will be stopped in a buffer gas cell in which Resonance Ionization Spectroscopy (RIS) is performed with detection of the ionization process by the α -decay of ^{254}No . The technique is similar to that developed for RIS on fission isomers [11]. To determine the stopping distribution of the 40 MeV No recoils, a 40 MeV $^{238}\text{U}^{8+}$ beam from the tandem van-de-Graaff accelerator at the MP-Tandem accelerator facility in Heidelberg was implanted in a buffer gas cell. The range distribution and the lateral straggling of the ions in the gas was measured for different gas pressures. The normalized count rate of the movable semiconductor detector is shown in Fig. 7 as a function of the distance from the entrance foil.

The code SRIM2000 predicts a 30% shorter range which might originate from assuming a too high effective charge state of the ions during the slowing-down process. Similar derivations between measurements and calculations have been found for the straggling. These results have been taken into account for the design of the buffer gas cell. The cell has been constructed, and first vacuum and high voltage tests have been carried out successfully [12].

Furthermore, we plan to study ion chemical reactions of heavy elements such as ^{254}No and ^{256}Lr in a buffer gas cell with well-defined admixtures, e.g. O_2 , H_2O , CH_4 , CO_2 .

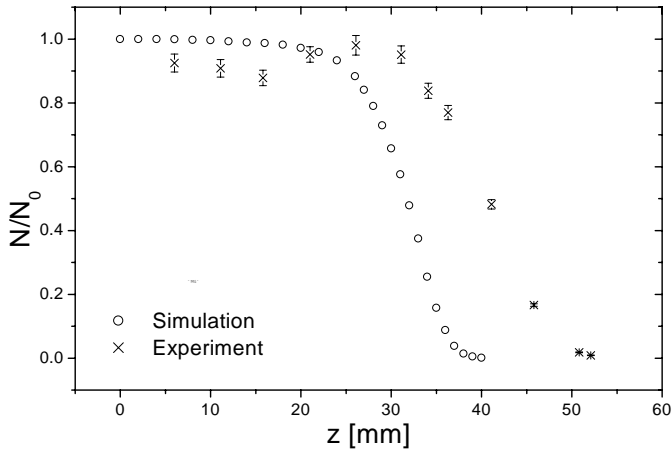


Figure 7: Range distribution of the U ions in Ar at a gas pressure of 250 mbar (\times). The calculation (\circ) is based on the code SRIM2000 [13].

The reaction products will be identified mass selectively by the Ion Guide Quadrupole Mass Separation (IGQMS) technique [14, 15]. Presently, we are working on establishing the method on chemically homologue elements.

In a first step, ion-molecule reactions will be studied with a Fourier Transform Mass Spectrometer (FT/MS) under well-defined experimental conditions [16]. In first experiments erbium reactions with O_2 have been investigated. The ions are created by laser ablation from a solid target using a pulsed CO_2 laser, cooled by an argon buffer gas push and stored in a FT-ICR cell at constant O_2 gas pressure. An ejection sweep cleans the cell from all ions with the exception of erbium ions which react with oxygen. The results are shown in Fig. 8. The ratio of Er^+ to ErO^+ intensity, as obtained after various reaction times, is shown in Fig. 9. From the exponential decay of the Er^+ signal a reaction constant can be deduced.

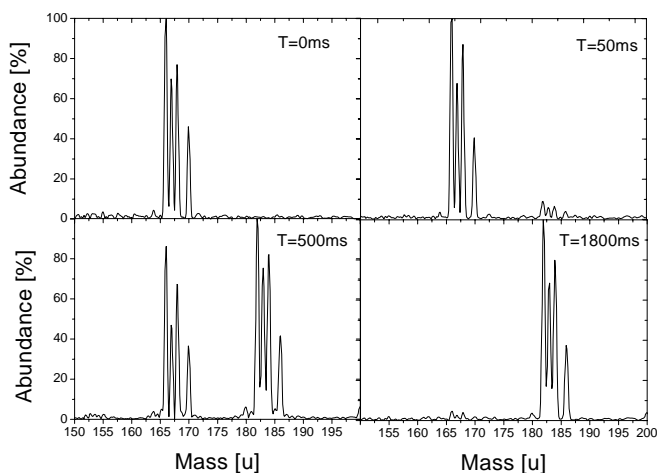


Figure 8: Er^+ and ErO^+ mass spectra at reaction time T as indicated. The groups around mass number 167 and 183 belong to Er^+ and ErO^+ , respectively.

In a second step the results from these FT-ICR experiments which are obtained under clean experimental conditions will be compared with results obtained in the inert

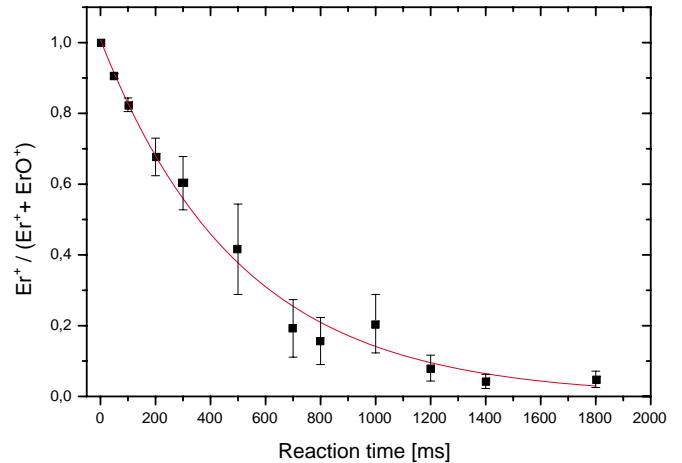


Figure 9: Intensity ratio of Er^+ to $(Er^+ + ErO^+)$ as function of the reaction time.

buffer gas cell to which the reaction gas is admixed. Energetic erbium ions from a Tandem van-de-Graaff accelerator will be implanted into the buffer gas cell. Ion-chemical reactions will be investigated in ‘hot’ and ‘cold’ surroundings. ‘Hot’ surrounding is expected if erbium thermalizes directly as an ion. If it thermalizes as an atom, which subsequently is resonantly ionized by the laser, the surrounding is ‘cold’.

Acknowledgement

We acknowledge financial support by the European Union (Networks EXOTRAPS and EUROTRAPS) and by BMBF under contract number 06 LM 973.

References

- [1] N. Hermanspahn et al., Phys. Rev. Lett. **84** (2000) 427.
- [2] H. Häfner et al., Phys. Rev. Lett. **85** (2000), 5308.
- [3] Thomas Beier, this annual report
- [4] F. Herfurth et al., 2001, Nucl. Instr. Meth. **A** (in print), available as GSI preprint 2000-14
- [5] H. Raimbault-Hartmann et al., Nucl. Instr. Meth. **B126** (1997), 378.
- [6] G. Bollen et al., Nucl. Instr. Meth. **A368** (1996), 675.
- [7] G. Münzenberg et al., Nucl. Instr. Meth. **161** (1979), 65.
- [8] O. Engels et al., Annual Report, GSI (1999)
- [9] R. Naaman et al., Rev. Sci. Instrum. **67** (1996), 3332.
- [10] V.L. Varentsov et al., Nucl. Instr. Meth. **A 413** (1998) 447.
- [11] H. Backe et al., Phys. Rev. Lett. **B 80** (1998), 920.
- [12] W. Ludolphs, Diploma Thesis, Inst. f. Kernphysik, Universität Mainz, (2001).
- [13] J.F. Ziegler et al., The Stopping and Range of Ions in Solids, Pergamon Press, New York, (1985), 488.
- [14] H. Backe et al., Nucl. Instr. Meth. **B 126** (1997), 406.
- [15] A. Iivonen et al., Phys. Scripta **42**, (1990), 133.
- [16] A.G. Marshall, L. Schweikhard, Int. J. Mass Spectrom. Ion Proc. **118/119** (1992), 37.

Mean-Field Instability of Trapped Ultracold Fermi Gases

R. Roth and H. Feldmeier (GSI)

The success in cooling a cloud of fermionic ^{40}K atoms, kept in a magnetic trap, to temperatures significantly below the Fermi energy [1,2] opened a unique possibility to study the properties of dilute degenerate Fermi gases experimentally. One long-term goal is the observation of a BCS phase transition in these systems. The mechanism to create Cooper pairs relies on an attractive interaction between the particles. At the same time these attractive interactions can cause a mean-field collapse of the metastable dilute Fermi gas towards high densities. Obviously a necessary prerequisite to reach the BCS transition is the stability of the normal Fermi gas.

We investigate the mean-field instability of the trapped Fermi gas in the framework of density functional theory. The energy density of the interacting multi-component Fermi gas is constructed in a mean-field picture using the Thomas-Fermi approximation. The interaction between the atoms is described by the s- and p-wave terms of the Effective Contact Interaction (ECI) [3,4], which depends on the s- and p-wave scattering length, a_0 and a_1 , resp., as well as on the s-wave effective volume b_0 . The ECI is constructed such that the exact two-body energy spectrum is reproduced by the expectation values of the ECI in mean-field type states.

The energy density of a single-component Fermi gas trapped in an external potential $U(\vec{x})$ reads

$$\mathcal{E}_1[\kappa(\vec{x})] = \frac{U(\vec{x})}{6\pi^2} \kappa^3(\vec{x}) + \frac{1}{20\pi^2 m} \kappa^5(\vec{x}) + \frac{a_1^3}{30\pi^3 m} \kappa^8(\vec{x}),$$

where $\kappa(\vec{x}) = \sqrt[3]{6\pi^2 \rho(\vec{x})}$ denotes the local Fermi momentum and a_1 the p-wave scattering length. The first term originates from the external potential, the second one from the kinetic energy, and the third term from the p-wave interaction. The s-wave part of the interaction does not contribute in a system of identical fermions due to the Pauli principle.

For attractive p-wave interactions, i.e., negative p-wave scattering length $a_1 < 0$, the highest power of $\kappa(\vec{x})$ in the energy density has a negative coefficient. This implies that there is a maximum density up to which the system is stable. Beyond this density the energy decreases for growing density and the system collapses towards a high density configuration. For fixed particle number N we obtain the following local condition for the stability of the single-component Fermi gas [3,4]

$$-a_1 \kappa(\vec{x}) \leq \sqrt[3]{3\pi}/2.$$

If this stability condition is violated anywhere in the trap then the system will collapse.

The energy density of a two-component Fermi gas, where we assume equal local Fermi momenta $\kappa(\vec{x}) = \kappa_1(\vec{x}) = \kappa_2(\vec{x})$ for both components, reads

$$\begin{aligned} \mathcal{E}_2[\kappa(\vec{x})] = & \frac{U(\vec{x})}{3\pi^2} \kappa^3(\vec{x}) + \frac{1}{10\pi^2 m} \kappa^5(\vec{x}) \\ & + \frac{a_0}{9\pi^3 m} \kappa^6(\vec{x}) + \frac{\tilde{a}_1^3}{10\pi^3 m} \kappa^8(\vec{x}) \end{aligned}$$

with $\tilde{a}_1^3 = a_1^3 + b_0/3$. In this case both, s- and p-wave interactions contribute and influence the stability of the system. We obtain the following stability condition for the two-component Fermi gas [3,4]

$$-a_0 \kappa(\vec{x}) - 2[\tilde{a}_1 \kappa(\vec{x})]^3 \leq \pi/2.$$

For practical purposes this stability condition can be rephrased in terms of an upper limit in the number of particles $N = N_1 = N_2$ assuming a parabolic trapping potential with mean oscillator length $\ell = 1/\sqrt{m\omega}$ [3,4]. Figure 1 shows the logarithm of the maximum particle number of each component as a function of the s- and p-wave scattering length in units of the mean oscillator length.

Attractive s-wave as well as attractive p-wave interactions can cause a mean-field collapse. If both components are attractive then their combined action decreases the maximum allowed density or particle number for the stable configuration. If one component is attractive and the other repulsive then the repulsive one stabilizes the system, i.e., increases N_{\max} . New phenomena appear in the case of attractive s-wave and repulsive p-wave interactions. If the p-wave scattering length exceeds about 1/3 of the s-wave scattering length (compare Fig. 1) the p-wave repulsion prevents a collapse completely, i.e., $N_{\max} \rightarrow \infty$. For p-wave repulsions slightly too weak to cause this absolute stabilization a novel high-density phase appears in the center of the trap if N_{\max} is exceeded.

We conclude that p-wave interactions have an important influence on the stability and may thus be helpful on the way to Cooper pairing in trapped ultracold Fermi gases.

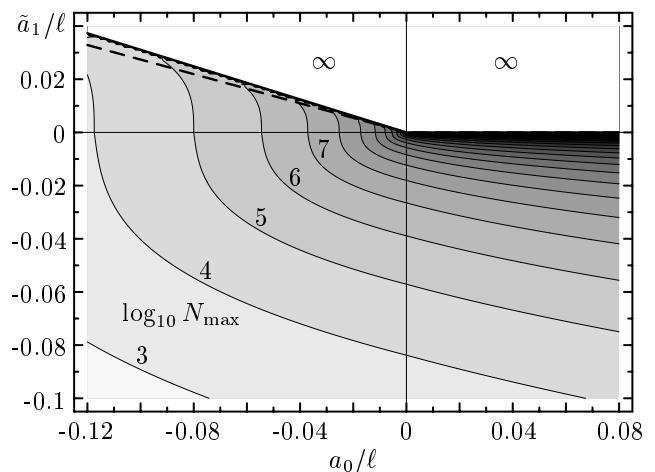


Fig. 1: Contour plot of the logarithm of the maximum particle number N_{\max} in a two-component Fermi gas as function of the s- and p-wave scattering lengths, a_0/ℓ and \tilde{a}_1/ℓ , where ℓ is the mean oscillator length of the trap.

- [1] B. DeMarco, D.S. Jin; Science 285 (1999) 1703.
 [2] B. DeMarco, S.B. Papp, D.S. Jin; e-print: cond-mat/0101445.
 [3] R. Roth, H. Feldmeier; e-print: cond-mat/0102416.
 [4] R. Roth, H. Feldmeier; J. Phys. B 33 (2000) 787.
 see also: <http://theory.gsi.de/~trap/>

Parity Violation effects in highly-charged ions

I. Bednyakov, G. Plunien, G. Soff, Technische Universität Dresden
 L.N. Labzowsky, St. Petersburg State University,
 A.V. Nefiodov, St.Petersburg Nuclear Physics Institute,

Parity-nonconserving (PNC) atomic effects originate from the electroweak interaction of atomic electrons with the nucleus via Z -boson exchange. Comparing experimental results with theoretical predictions of the standard model allows to search for "new physics" beyond the standard model (e.g., a second Z -boson or new fermions) [1].

In the case of neutral atoms here is the discrepancy between theoretical and experimental results for PNC effects in the case of neutral atoms that might be explained by the uncertainties in the calculations caused by the inter-electronic interactions, correlation effects etc.

In highly-charged ions (HCI), on the other hand, the binding to the nucleus dominates by far the electron-electron interaction. The spin-independent part of an effective weak interaction Hamiltonian mediated by a Z -boson exchange is given by

$$\hat{H}_W(\mathbf{r}) = -\frac{G_F}{2\sqrt{2}} Q_W \rho_N(\mathbf{r}) \gamma_5, \quad (1)$$

where G_F is the Fermi constant, $\rho_N(r)$ is the nuclear density and γ_5 is the Dirac matrix. Due to this effective Hamiltonian states with opposite parity will be admixed. The transition amplitudes of a given atomic processes can be expressed as:

$$A = A_0 + i\eta A_1, \quad (2)$$

where A_0 denotes the amplitude of the basic process and A_1 is the amplitude being related to parity violation.

Electroweak-radiative corrections were considered both for neutral atoms (e.g. see Ref. [2] and also for hydrogen-like ions [3]. The consideration of these radiative corrections becomes necessary because they can contribute up to 10% of the total magnitude of PNC effects.

For experiments, a promising situation occurs in He-like ions due to the near-degeneracy of two levels with opposite parities, 2^1S_0 and 2^3P_0 near $Z = 64$ (Gd^{62+}) as well as close to $Z = 92$ (U^{90+}). The situation has been analyzed in Gd^{62+} and Eu^{61+} . In particular we propose a quenching-type experiment with an interference of hyperfine- and weak-quenched transitions [4].

A typical situation for parity violation in atoms concerns the $M1$ transition with an admixture of the $E1$ transition. The one-photon hyperfine-quenched transition $2^1S_0 \rightarrow 1^1S_0$, via emission of a magnetic photon ($M1$), is due to the hyperfine mixing of the 2^1S_0 and 2^3S_1 levels. The weak interaction of electrons opens another one-photon decay channel $2^1S_0 \rightarrow 1^1S_0$, via the $E1$ emission through the mixing of the 2^1S_0 and 2^3P_1 levels by the operator \hat{H}_W . As a result, the total amplitude A in Eq. (2) appears as a mixture of the basic $M1$ amplitude $A_0 \equiv A_s$ and of the additional $E1$ amplitude $A_1 \equiv A_p$. The corresponding transitions rates are W_s and W_p , respectively. The weak mixing coefficient η is determined by

$$i\eta\Delta_0 = \langle 2^3P_0 | \hat{H}_W | 2^1S_0 \rangle, \quad (3)$$

where $\Delta_0 = E_{2^1S_0} - E_{2^3P_0}$. The theoretical predictions

Nucl.	$W_s(\text{s}^{-1})$	$W_p(\text{s}^{-1})$	η
${}_{63}^{151}\text{Eu}$	0.68×10^8	0.11×10^{14}	0.33×10^{-6}
${}_{64}^{155}\text{Gd}$	0.58×10^6	0.75×10^{11}	0.91×10^{-6}

for these quantities in europium and gadolinium are listed in the Table. Due to the admixture of states of opposite parity, in a polarized-beam experiment a small asymmetry in the number of emitted photons per direction should become visible, expressed by

$$dW(\mathbf{n}) = \frac{W_s}{4\pi} [1 + \varepsilon(\boldsymbol{\zeta} \cdot \mathbf{n})] d\Omega \quad (4)$$

where \mathbf{n} indicates the direction of the photon emission and $\boldsymbol{\zeta}$ is the unit vector in direction of the polarization of the ion. The coefficient of asymmetry is given by $\varepsilon = 3\lambda_0\eta R/(I+1)$ with $R = \sqrt{W_p/W_s}$. Here $\lambda_0 \leq 1$ denotes the degree of polarization.

The total asymmetry effect turns out to be $\varepsilon \simeq 0.37\lambda_0 \times 10^{-3}$ for Gd^{62+} , which is unusually large for parity-violation effects, but the lifetime of the 2^1S_0 level is about one order of magnitude smaller than the hyperfine-quenched 2^3P_0 lifetime. This implies a strong background in experiments with Gd^{62+} .

In Eu^{61+} the weak asymmetry effect reduces to $\varepsilon \simeq 0.11\lambda_0 \times 10^{-3}$, but the 2^1S_0 level lives significantly longer than the hyperfine-quenched 2^3P_0 level.

Since photons being observed in this experiment originate from single-photon decays of the hyperfine- and weak-quenched $F = I$ state, the success of the experiment will depend crucially on the production of a significant degree of polarization for this state of the He-ion. This is a task to be achieved experimentally in order to exploit the advantages of highly-charged ion investigations for parity-violation effects.

References

- [1] G. Soff, I. Bednyakov, T. Beier, F. Erler, I. Goidenko, U. Jentschura, L. N. Labzowsky, A. Nefiodov, G. Plunien, R. Schützhold, and S. Zschocke. "Effects of QED and beyond from the atomic binding energy" (APAC2000 Conference), "Hyperfine Interactions"
- [2] B. W. Lynn and P. G. H. Sandars, J. Phys. B **27**, 1469 (1994).
- [3] I. Bednyakov, L. Labzowsky, G. Plunien, G. Soff, and V. Karasiev, Phys. Rev. A **61**, 012103 (1999).
- [4] L. N. Labzowsky, A. V. Nefiodov, G. Plunien, G. Soff, R. Marrus, and D. Liesen. *preprint 2000* "Parity-violation effect in heliumlike gadolinium and europium"

Divergence of Perturbation Theory and Resummation

Ulrich Jentschura and Gerhard Soff

TECHNISCHE UNIVERSITÄT DRESDEN, 01062 DRESDEN

Current determinations of fundamental constants [1] and the comparison of theory and experiment in high-precision experiments are based on perturbative expansions which can at best be regarded as divergent, asymptotic series in the coupling constant [2]. The first terms of the series decrease in absolute magnitude, before the factorial growth of the perturbative coefficients overcompensates the additional coupling factors of higher orders in perturbation theory, and the perturbation series ultimately diverges. Dyson's related argument [3] has given rise to much discussion and confusion, until recent explicit 30-loop calculations of perturbation series pertaining to ϕ^3 and Yukawa theories have firmly established the factorially divergent character of the perturbative expansion [4]. These considerations naturally lead to the question of how complete, nonperturbative results can be obtained from a finite number of perturbative coefficients, and how the nonperturbative result is related to the partial sums of the perturbation series.

We have investigated this problem [5] in connection to the Euler-Heisenberg-Schwinger effective Lagrangian which describes the quantum electrodynamic corrections to Maxwell's equations. The forward scattering amplitude of the vacuum ground state is described by a factorially divergent asymptotic series, $S_B \propto \text{const.} \times g_B \sum_{n=0}^{\infty} c_n g_B^n$. The expansion coefficients

$$c_n = \frac{(-1)^{n+1} 4^n |\mathcal{B}_{2n+4}|}{(2n+4)(2n+3)(2n+2)},$$

where \mathcal{B}_{2n+4} is a Bernoulli number and g_B is the coupling, display an alternating sign pattern and grow factorially in absolute magnitude. The process by which a finite, nonperturbative result is ascribed to a divergent perturbation series is known as *resummation*. The resummation to the complete nonperturbative result for S_B is accomplished by employing the delta transformation,

$$\delta_n^{(0)}(\beta, s_0) = \frac{\sum_{j=0}^n (-1)^j \binom{n}{j} \frac{(\beta+j)_{n-1}}{(\beta+n)_{n-1}} \frac{s_j}{a_{j+1}}}{\sum_{j=0}^n (-1)^j \binom{n}{j} \frac{(\beta+j)_{n-1}}{(\beta+n)_{n-1}} \frac{1}{a_{j+1}}},$$

where $s_n = \sum_{k=0}^n a_k$ is the partial sum of the input series and $a_j = c_j g^j$ is the j th term in the perturbation series; $(a)_m = \Gamma(a+m)/\Gamma(a)$ is a Pochhammer symbol. It has been observed that the delta transformation can be used under rather general assumptions for the extrapolation of the perturbation series, i.e. the prediction of unknown perturbative coefficients, and various applications to phenomenologically important quantum field theoretic perturbation series have been presented in [5,6]. In many cases, the delta transformation leads to better results than Padé approximants which have been discussed abundantly in the literature (see e.g. [7]).

A perturbation series often misses physically important physical effects when interpreted "at face value". For example, the perturbative expansion describing the energy shift of hydrogenic levels in an electric field (known as the Stark effect) has purely real coefficients, whereas the complete energy eigenvalue (more precisely, pseudoeigenvalue or resonance) also has an imaginary component. The imaginary part of the resonance, which describes the autoionization width, can be obtained from the purely real perturbation series by a transformation which can be characterized as a generalized Borel summation [8,9]. First, the factorial growth of the perturbation series is divided out by calculating the Borel transform, and the perturbation series $f(g) = \sum_n c_n g^n$ is replaced by its Borel transform $\mathcal{B}(g) = \sum_n c_n g^n/n!$. Then, the autoionization width is obtained by integrating the Borel transform in the complex plane along integration contours specified in [9,10]. The same resummation procedure can be used to obtain the quantum electrodynamic pair production amplitude for the case of an electric field background; the pair-production amplitude is related to the imaginary part of the effective action [10].

Recently, techniques have been investigated to accelerate the convergence of resummation procedures in order to obtain results even at large coupling, which are paradoxically based on the weak-coupling perturbative expansions [11]. The extrapolation from the weak-coupling limit to the regime of strongly coupled systems by analytic continuation of the perturbation series via Borel or delta transformations has wide applicability.

References

- [1] P. J. Mohr and B. N. Taylor, Rev. Mod. Phys. **72**, 351 (2000).
- [2] J. Zinn-Justin, *Quantum Field Theory and Critical Phenomena*, 3rd ed. (Clarendon Press, Oxford, 1996).
- [3] F. J. Dyson, Phys. Rev. **85**, 631 (1952).
- [4] D. Broadhurst and D. Kreimer, Phys. Lett. B **475**, 63 (2000).
- [5] U. D. Jentschura, J. Becher, E. J. Weniger, and G. Soff, Phys. Rev. Lett. **85**, 2446 (2000).
- [6] U. D. Jentschura, E. J. Weniger, and G. Soff, J. Phys. G **26**, 1545 (2000).
- [7] M. A. Samuel, J. Ellis, and M. Karliner, Phys. Rev. Lett. **74**, 4380 (1995).
- [8] V. Franceschini, V. Grecchi, and H. J. Silverstone, Phys. Rev. A **32**, 1338 (1985).
- [9] U. D. Jentschura, e-print physics/0010038 (Phys. Rev. A, in press).
- [10] U. D. Jentschura, Phys. Rev. D **62**, 076001 (2000).
- [11] U. D. Jentschura and G. Soff, J. Phys. A **34**, 1451 (2001).

The g factor of an electron bound in hydrogenlike ions - status of the theoretical predictions

Thomas Beier, *Gesellschaft für Schwerionenforschung, Darmstadt, Germany*

For only few fundamental physical quantities experiment [1] and theory [2] agree that well as for the g factor of the free electron. It can therefore be considered as a precision test of quantum electrodynamics (QED) for free particles. To test QED also in the presence of strong electric fields, measurements on the g factor of an electron bound in a hydrogenlike system are one possible way. In $^{12}\text{C}^{5+}$, a value of $g = 2.001\,041\,596(5)$ was measured [3] which has to be compared to the theoretical prediction of $g = 2.001\,041\,591(7)$ [4]. This measurement is therefore the most stringent comparison of QED theory and experiment in any system heavier than hydrogen up to now. The major uncertainty of the experimental value results from the mass ratio $m_e/m_{^{12}\text{C}^{5+}}$, taken from [5], and an only slight improvement in the theoretical precision would allow to determine the electron mass more accurately. Here, the current limits to theory are presented and discussed.

The value given in [4] includes the g factor of the free electron including all QED corrections to that value, and in addition the corrections due to the binding to a heavy nucleus:

1. the binding correction itself which can be characterized as a transition from the spin quantum number to the total angular-momentum quantum number that is the only observable in a central field. It describes the deviation of g from the Dirac value of 2 for the free electron and is given by $g_j = (2/3)[1 + 2\sqrt{1 - (Z\alpha)^2}]$ for the 1s state. This applies only to point-like nuclei. For extended nuclei, the wave function of the electron is slightly modified.

2. The finite nuclear-size correction which takes into account the extension of the nucleus is about 4×10^{-10} for carbon but amounts up to 1×10^{-3} for uranium where the uncertainty of the nuclear radius itself affects the prediction already on the 10^{-7} level.

3. The not-infinite nuclear mass causes the nucleus to move itself when orbited by the electron. A correct relativistic treatment has to consider nuclear recoil to all orders in the coupling constant $Z\alpha$ where Z is the charge of the nucleus. The exact form of this correction is not yet known and an existing expansion in $Z\alpha$ [6,7] yields reliable results only for light systems. For carbon it amounts to 87.5×10^{-9} with an estimated uncertainty of 1 % because of the expansion. This uncertainty should be considered to be 10 % of the value already for calcium. The complete relativistic recoil correction was calculated only for the Lamb shift up to now [8] and it seems to be much more complex for the g factor and the hyperfine structure splitting.

4. Another quantity connected with nuclear properties is that of nuclear polarization, i.e., the virtual excitation of nuclear degrees of freedom by exchange of at least two virtual photons with the electron. For the g factor, no investigations were carried out up to now. The works of G. Plu-

nien and G. Soff [9] deal with the influence on the Lamb shift in the approximation of Coulomb-photon exchange, and only recently the problem of transverse-photon exchange which is crucial for magnetic interactions was considered at least for the Lamb shift case [10]. However, we expect this effect to be even weaker than for the Lamb shift because the typical matrix element for g factor measurements is $\langle r \rangle$, compared to $\langle 1/r \rangle$ for the Lamb shift, and therefore the inner parts of the electronic wave function that contribute most to the nuclear polarization are less pronounced. It should be mentioned that this is *not* the case for the hyperfine structure splitting where the typical matrix element is given by $\langle 1/r^2 \rangle$. In that case, however, the effect is screened by other nuclear uncertainties (for a recent overview see [11]).

5. The most interesting quantities related to the g factor are the bound-state QED corrections. Those of first order in (α/π) (i.e. one virtual photon line in the corresponding Feynman diagram) are depicted in Fig. 1. They were eval-

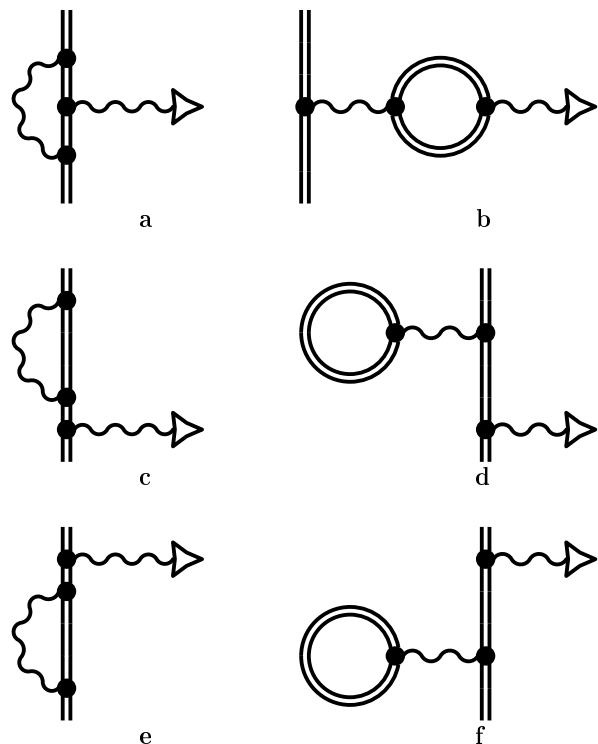


Fig. 1. Feynman diagrams representing the QED contributions of order (α/π) to the g factor of a bound electron. The wavy lines denote photons, which mediate the interaction with the external magnetic field represented by a triangle. In each diagram there is also one virtual photon. The solid double line indicates the electron and on the right side also virtual leptons in the electron-positron loops. The diagrams on the left are the self-energy-like corrections, those on the right the vacuum-polarization-like corrections. For the free electron, only the diagram similar to diagram a contributes.

uated in detail to all orders in $Z\alpha$ in [4]. They contain also the contribution to the g factor of the free electron of the same order, given by $\alpha/\pi \approx 2.323 \times 10^{-3}$. For comparison, the effect of binding in C^{5+} amounts only to 8.442×10^{-7} . In uranium the binding effect is 3×10^{-3} and therefore in particular heavy systems form an excellent base for investigations of bound-state QED.

The QED corrections of second order in (α/π) were never investigated beyond the first term in the $Z\alpha$ expansion. It can be shown for *all* orders of (α/π) that the leading term of the corresponding $Z\alpha$ expansion is given by $2 \times A^{(n)} \times (Z\alpha)^2/6$ where $A^{(n)}$ is the expansion coefficient for the n th power of (α/π) in the series for $g_{\text{free}}/2$ [12], i.e., $A^{(1)} = 1/2$. The next term in the $Z\alpha$ expansion is at least of the order $(Z\alpha)^4$, and therefore the $Z\alpha$ expansion allows to estimate the bound-state $(\alpha/\pi)^2$ contributions with an uncertainty of about 50 % for the case of carbon. This uncertainty increases rapidly for increasing Z , and we expect the error to be at least 100 % in the case of calcium already, where the leading term of the expansion for the first order in (α/π) already deviates for about 70 % from the non-perturbative value. The whole set of 50 diagrams for the order $(\alpha/\pi)^2$ is shown in Fig. 2. For the order $(\alpha/\pi)^3$, the number of diagrams exceeds 500. The 50 diagrams shown in Fig. 2 can be obtained by fixing the magnetic interaction to each point of the 10 diagrams contributing to the Lamb shift of order α^2 in hydrogenlike atoms (e.g., [13]). The calculation is slightly more complex because for each diagram the magnetic interaction and one additional electron propagator with the corresponding integration has to be considered. As there are problems already for some of the Lamb-shift diagrams, an evaluation of the set shown in Fig. 2 can not be expected without considerable effort. In particular, the diagrams that contribute most to the g factor in lighter systems are those with two self-energy loops in the upper rows of Fig. 2, and unfortunately exactly their counterpart, the so-called two-loop self-energy graphs, cause the major problems in the recent calculations for the Lamb shift (e.g., [14] and references therein). The situation would be different in muonic atoms where the vacuum-polarization contributions are strongly enhanced compared to those from self-energy-like graphs. An additional experiment on a muonic system therefore could provide valuable additional information. However, in muonic systems the nuclear polarization can be expected to be as large as the QED corrections of order (α/π) .

All theoretical contributions to the g factor of the electron bound in hydrogenlike carbon are given in Table 1. Together with the experimental value, this leads to an independent new value for the electron mass [15], $m_e = 5.485\,799\,092 \times 10^{-3}$ u. A detailed discussion about the corresponding measurement and evaluation procedure is to be found elsewhere in this report [16].

We want to thank S. G. Karshenboim, K. Pachucki, V. M. Shabaev, and V. A. Yerokhin for valuable discussions.

- [1] R. S. Van Dyck Jr. *et al.*, PRL 59 (1987) 26.
- [2] A. Czarnecki and W. J. Marciano, Nuc. Phys. B (Proc. Suppl.) 76 (1999), 245.
- [3] H. Häffner *et al.*, PRL 85 (2000) 5308.

- [4] T. Beier *et al.*, PRA 62 (2000) 032510.
- [5] D. L. Farnham *et al.* PRL 75 (1995) 3598.
- [6] R. Faustov, Nuovo Cimento LXIX A, No. 1 (1970) 37; Phys. Lett. 33B (1970), 422.
- [7] H. Grotch, PRA 2 (1970) 1605; H. Grotch and R. A. Hegstrom, PRA 4 (1971) 59.
- [8] V. M. Shabaev, PRA 57 (1998) 59; V. M. Shabaev *et al.*, PRA 57 (1998) 4235.
- [9] G. Plunien and G. Soff, PRA 51 (1995) 1119; PRA 53 (1996) 4614, and references therein.
- [10] N. Yamanaka *et al.*, Hyp. Int. 127 (2000) 297.
- [11] T. Beier, Phys. Rep. 339 (2000) 79.
- [12] A. Czarnecki *et al.*, Phys. Rev. A 63 (2001) 012509.
- [13] P. Mohr *et al.*, Phys. Rep. 293 (1998) 227.
- [14] V. A. Yerokhin, PRL 86 (2001) 1990, and refs. therein.
- [15] G. Werth *et al.*, Hyp. Int., in print.
- [16] W. Quint *et al.*, Contribution to this annual report.

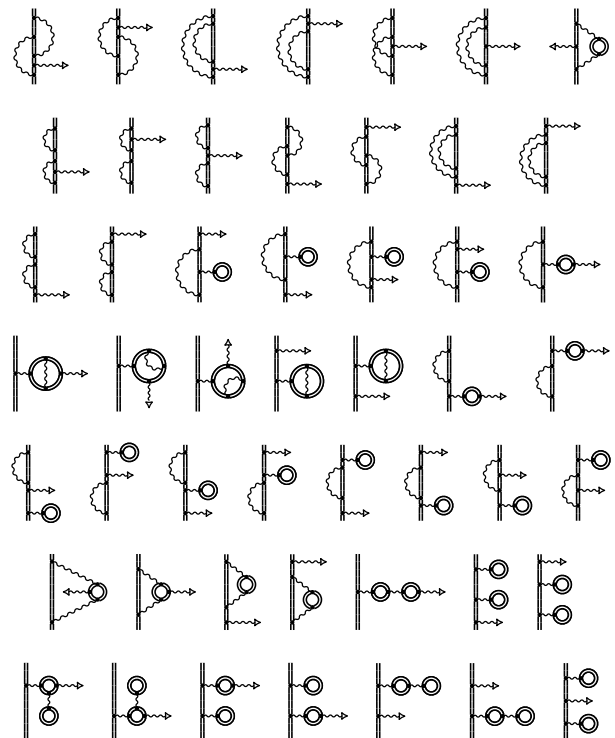


Fig. 2. Diagrams contributing to order $(\alpha/\pi)^2$ to the g factor of a bound electron. Only seven diagrams of this order have to be considered for the g factor of a free electron, similar to these of the first row.

Table 1. Known theoretical contributions to the g factor of an electron bound in the ground state of $^{12}C^{5+}$. All values are given in units of 10^{-9} . If no error is given, it is less than 0.5×10^{-10} . The error for the “total” value is a linear addition of the three errors given in order not to underestimate any systematic effect.

Contribution	numerical value (in 10^{-9})
binding	1 998 721 354.2
fin. nuc. size	0.4
recoil	87.5(9)
free QED, order (α/π) :	2 322 819.6
bound QED, order (α/π) :	844.3(12)
free QED, $(\alpha/\pi)^2$ to $(\alpha/\pi)^4$	-3 515.1
bound QED, $(\alpha/\pi)^2$ $(Z\alpha)^2$	-1.1(5)
total:	2 001 041 589.8(26)

Interelectronic-interaction effect on the radiative recombination of an electron with a heavy He-like ion

V.A. Yerokhin ^{a,b,c}, V.M. Shabaev ^{a,b,c}, T. Beier ^b, and J. Eichler ^c

^a St.Petersburg State University, St.Petersburg, Russia

^b Gesellschaft für Schwerionenforschung (GSI), Darmstadt, Germany

^c Hahn-Meitner Institut Berlin, Germany

In energetic atomic collisions between highly charged high- Z ions and low- Z target atoms, radiative electron capture (REC) is one of the most important reaction channels. In the limit of a loosely bound target electron, REC is identical with radiative recombination (RR). Reactions of this type have been extensively studied in recent years for heavy highly charged projectiles up to bare uranium. The relativistic theory of REC in the one-electron approximation is well established at present ([1] and references therein), and results of numerical calculations are in excellent agreement with experiment [2]. While radiative recombination of an electron with a bare nucleus is well understood theoretically, the process involving an ion with several electrons is complicated by the interelectronic interaction. The REC process into the L-shell of He-like uranium was measured in [3].

We systematically investigated the interelectronic-interaction effect on radiative recombination of an electron with a heavy He-like ion. Here, the number of electrons ($N=3$) is much smaller than the nuclear charge number Z and therefore their mutual interaction is by a factor $1/Z$ smaller than that with the Coulomb field of the nucleus. To zeroth approximation, the interelectronic-interaction can be neglected and thus the process is equivalent to RR of an electron with a bare nucleus, studied thoroughly in [1]. Here, we investigated the correction of first order in $1/Z$ due to the interelectronic interaction.

We consider RR of an electron with a definite momentum and polarization with a heavy He-like atom in the ground state located at the origin of the coordinate frame. The final state of the system is a Li-like ion in the state $(1s)^2v$, where v denotes a valence electron. The first-order (in $1/Z$) interelectronic-interaction correction to the process under consideration can be represented by a set of Feynman diagrams shown in Fig. 1. Here, the operator

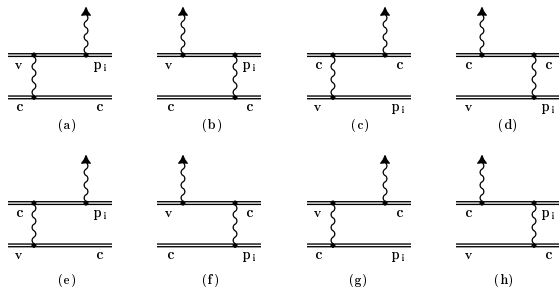


Fig. 1. Feynman diagrams representing the interelectronic-interaction corrections of first order in $1/Z$ to radiative recombination of an electron with a He-like atom. \mathbf{p}_i denotes the incoming electron in the continuum spectrum, \mathbf{v} and \mathbf{c} indicate the valence and the core electrons, respectively. The line terminated by a triangle represents the emitted photon.

Table 1. Zeroth-order total cross section $\sigma^{(0)}$ and the first-order interelectronic-interaction correction in different evaluations, in barns. $\sigma_{\text{zeff}}^{(1)}$ denotes the interelectronic-interaction correction calculated in the effective-nuclear-charge approximation with parameter $Z_{\text{eff}} = 90.3$, $\sigma_{\text{scr}}^{(1)}$ corresponds to the screening-potential approximation, $\sigma_{\text{int}}^{(1)}$ indicates the results of the rigorous relativistic treatment.

E [Mev/u]	$\sigma^{(0)}$	$\sigma_{\text{zeff}}^{(1)}$	$\sigma_{\text{scr}}^{(1)}$	$\sigma_{\text{int}}^{(1)}$	
10	504.65	-17.390	-19.635	-21.392	
2s _{1/2}	100	41.203	-1.880	-1.393	-2.055
700	2.457	-0.1768	-0.0979	-0.1051	
10	656.95	-38.523	-34.978	-35.396	
2p _{1/2}	100	33.041	-2.975	-2.535	-3.088
700	1.065	-0.1336	-0.1022	-0.0861	
10	854.82	-38.620	-39.671	-40.008	
2p _{3/2}	100	31.489	-2.259	-2.275	-2.896
700	0.622	-0.0600	-0.0568	-0.0489	

of the photon emission and the operator of the electron-electron interaction are combined in all possible ways. We evaluate these diagrams directly, including the summation over the whole spectrum of the Dirac equation and the full electron-electron interaction that consists of the Coulomb, Breit and retarded parts. The details of the derivation are given in [4]. Here, we present the results of the evaluation.

The numerical results for the interelectronic-interaction correction to the total RR cross section of an electron with He-like uranium are presented in Table 1. The calculation is carried out for projectile energies of 10-700 MeV per nuclear mass unit. The results of the rigorous relativistic treatment are compared with the calculations based on an effective-nuclear-charge approximation and on the screening-potential approximation (for a discussion cf. [5]). The comparison shows a decreasing accuracy of the approximate methods for increasing projectile energy. On average, the screening-potential approximation is found to be more reliable than the effective-nuclear-charge approximation. Its typical deviation from the rigorous treatment is about 10 – 20 % of the interelectronic-interaction correction, i.e., about 1 – 2 % of the cross section of the process. Therefore, fully relativistic calculations are needed to obtain an accuracy better than a few percent of the cross section of the process.

We want to thank Th. Stöhlker for valuable discussions. Financial support by DFG and RFBR is gratefully acknowledged.

- [1] J. Eichler and W. Meyerhof, *Relativistic Atomic Collisions*, Academic Press, San Diego, 1995.
- [2] Th. Stöhlker *et al.*, Phys. Rev. Lett. 82 (1999) 3232.
- [3] Th. Stöhlker *et al.*, Phys. Rev. Lett. 73 (1994) 3520.
- [4] V. A. Yerokhin *et al.*, Phys. Rev. A 62 (2000) 042712.
- [5] V. A. Yerokhin *et al.*, Hyp. Int, in print.

Resonant Transfer and Excitation for H- and He-like U-Ions

Zoltán Harman, Stephan Zakowicz, Matthias Gail, Norbert Grün, Werner Scheid
 Institut für Theoretische Physik, Justus-Liebig-Universität Giessen

We present calculations for the angular distribution of photons emitted after KLL-RTE (Resonant Transfer and Excitation) in collisions of U^{91+} - and U^{90+} -ions with hydrogen atoms. Measurements with H-like projectiles were recently performed by Ma et al. at GSI and are currently being evaluated [1]. In the past, a similar process has been studied both experimentally [2] and theoretically [3], in which graphite was used as target. However, the width of the Compton profile of the electron bound in the H-atom is smaller than in graphite, resulting in a better resolution of the resonance groups in the cross sections.

The electron bound in the hydrogen atom can be regarded as quasifree. Therefore, the RTE cross section can be calculated by using the cross section of dielectronic recombination (DR). In DR, a free electron is captured by the projectile with the simultaneous excitation of a bound electron, followed by the emission of a photon. Doubly-excited states embedded in the one electron continuum give rise to resonances in the cross sections. With perturbation theory we obtain the following expression for the differential cross section in the rest frame of the projectile ion:

$$\frac{d\sigma_{i \rightarrow d \rightarrow f}^{DR}}{d\Omega_k} = \frac{2\pi}{F_i} \frac{1}{2(2J_i + 1)} \sum_{M_f \lambda} \sum_{M_d} \sum_{M_i m_s} |\langle \Psi_d; J_d M_d | V_{capt.} | \Psi_i; J_i M_i, p_e m_s \rangle|^2 \times \frac{|\langle \Psi_f; J_f M_f, \mathbf{k} \lambda | H_{er} | \Psi_d; J_d M_d \rangle|^2}{(E - E_d)^2 + \Gamma_d^2/4} \rho_f.$$

This formula makes use of the isolated resonance approximation, in which interference effects between the intermediate states are neglected. The first matrix element describes the resonant capture of the free electron, where the operator $V_{capt.}$ is the sum of the Coulomb- and Breit-interaction operators. The second matrix element describes the radiative transition. The differential cross section can be expressed by means of the total cross section:

$$\frac{d\sigma_{i \rightarrow d \rightarrow f}^{DR}}{d\Omega_k} = \frac{\sigma_{i \rightarrow d \rightarrow f}^{DR}}{4\pi} (1 + \beta P_2(\cos \theta)),$$

where θ denotes the angle of emission of the photon with respect to the direction of the incoming electron. The anisotropy parameter β depends on the matrix elements for resonant capture and on the total angular momenta of the intermediate and final states.

In order to obtain the cross section for RTE in the impulse approximation, the cross section for DR is convoluted with the probability density of the target electron in momentum space:

$$\frac{d^2 \sigma_{RTE}}{d\Omega d\omega} = \int d^3 q' \frac{d\sigma_{DR}(\mathbf{q})}{d\Omega} |\phi_i(\mathbf{q}')|^2 \delta(\omega + E_f - e_i - E_i).$$

Here, $\phi_i(\mathbf{q}')$ denotes the Fourier transform of the wave function of the target electron in the target frame. The δ -function ensures the conservation of energy.

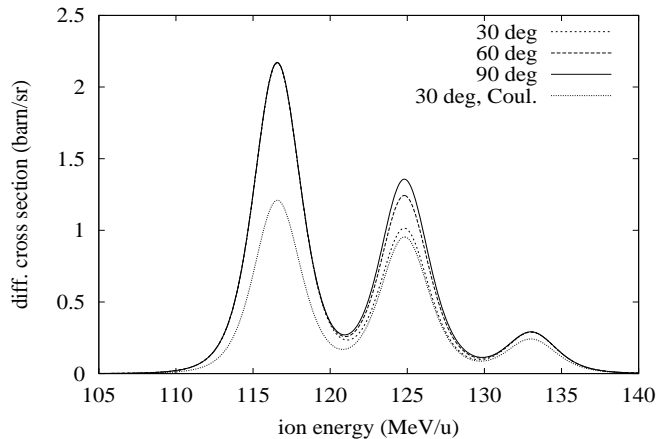


Figure 1: Differential cross sections for KLL-RTE in U^{91+} in the projectile frame at the angles $\theta = 30^\circ, 60^\circ$ and 90° .

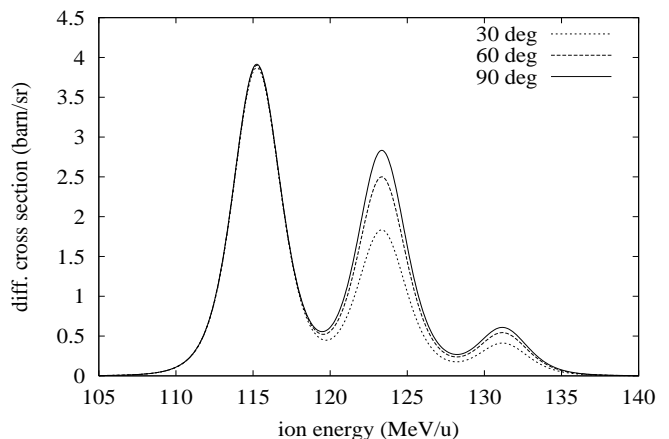


Figure 2: Differential cross sections for KLL-RTE in U^{90+} at the same angles.

Fig. 1 shows differential cross sections in the projectile system at different angles for U^{91+} -ions scattered on hydrogen atoms. The radiation has a strong angular dependence for energies in the range of the $KL_{1/2}L_{3/2}$ resonance group, while it is nearly isotropic for the other two resonance groups $KL_{1/2}L_{1/2}$ and $KL_{3/2}L_{3/2}$. The lowest curve was obtained by neglecting the effects of the Breit interaction.

The case of U^{90+} -ions is shown in Fig. 2. The cross section is anisotropic in the $KL_{1/2}L_{3/2}$ and $KL_{3/2}L_{3/2}$ groups. Also the cross sections are larger than the ones for the H-like projectile ions.

References

- [1] X. Ma et al., this report (2001)
- [2] T. Kandler et al., *Phys. Lett. A* **204** 274 (1995)
- [3] M. Gail et al., *J. Phys. B* **31** 4645 (1998)

Hyperfine Splitting of Hydrogenlike Thallium

M. Tomaselli ^{a,b}, T. Kühl ^b, W. Nörtershäuser ^b, D. Marx ^b, S. Borneis ^b, A. Dax ^b, H. Wang ^b,
and S. Fritzsche ^c

^a University of Darmstadt, ^b GSI Darmstadt, ^c University of Kassel

The investigation of hydrogenlike highly-charged ions is of interest for nuclear as well as for atomic physics. Measuring the ground-state hyperfine structure (HFS) splittings of these ions is a sensitive method to explore QED in extremely strong electric and magnetic fields and nuclear contributions to the electron energy. However, for a theoretical interpretation of the results it is necessary to separate the different contributions. Nuclear models have to provide charge and magnetization distributions of nuclei, which lead to the Breit-Rabi and the Bohr-Weisskopf effect, respectively, and corrections to the electron energy have to be calculated with QED. Interest was first focussed on the isotopes $^{207}\text{Pb}^{81+}$ and $^{205}\text{Bi}^{82+}$, where the theoretical description is simplified since they differ only by one nucleon from doubly-magic ^{208}Pb . The hyperfine structure of these isotopes was measured at GSI with laser spectroscopy at the ESR [1]. More recently, the hyperfine structure of $^{165}\text{Ho}^{66+}$, $^{185}\text{Re}^{74+}$, and $^{187}\text{Re}^{74+}$ was obtained by passive photon-emission spectroscopy in a high-energy electron-beam ion trap (SuperEBIT) at Livermore [2]. Similar experiments are presently under preparation to determine the HFS of thallium isotopes [3].

Previously, we applied the Dynamic Correlation Model (DCM) [4] to the hydrogenlike ions $^{207}\text{Pb}^{81+}$, $^{205}\text{Bi}^{82+}$, $^{165}\text{Ho}^{66+}$, and $^{185,187}\text{Re}^{74+}$ to derive the nuclear part in the HFS and combined the results with QED corrections [5]. The calculated hyperfine splittings are summarized in Table 1 and compared with other theoretical expectations [6, 7, 8] and experimental data. It turned out that the pure DCM results agree well with the experimental data, while adding the QED corrections led to a systematic deviation between theory and experiment. This is in contrast to the good description of nuclear properties by the dynamic correlation model and has motivated the application of the DCM to predict the HFS of the hydrogenlike thallium isotopes $^{203,205,207}\text{Tl}^{80+}$. The results are also included in Table 1. Besides, these calculations may guide future experiments at the GSI storage ring since an accurate *a priori* knowledge of the HFS transition frequency is required to avoid prohibitive large scan ranges.

In the DCM three terms contribute to the HFS: The first term is due to the single-hole magnetization, the second term was introduced in perturbative theory and describes spin-flip excitations [9], and the third term allows for collective correlation effects in the nucleus [5], it corresponds to higher-order perturbation diagrams. Taking these three terms into account the calculations accurately reproduce the experimental HFS. The systematic discrepancy to experimental data, which is observed after adding the QED corrections, might be the result of a double counting effect: The DCM calculations include “de facto” virtual mesons, which can decay into e^+e^- pairs, and these might be considered in radiative corrections as well. Another possibility is that the nuclear correlations, which are not taken into

account in QED calculations, have a distinct influence on the radiative corrections. Hence, the central question is how to compare the DCM terms and the radiative corrections of Refs. [10, 11]. The importance of this problem is evident: In the extreme single-particle model, QED and nuclear-magnetization corrections for high- Z atoms are of the same order of magnitude. Thus, the feasibility of testing the QED corrections depends strongly on the accuracy of the model used to evaluate the nuclear magnetization.

Table 1: Wavelengths of transitions between the ground state HFS components in hydrogenlike ions as calculated in the DCM and after combination with QED corrections taken from [11]. For comparison other theoretical and experimental data is given. All values in nm.

Ion	Theory			Exp.
	DCM	+QED	Other	
$^{165}\text{Ho}^{66+}$	572.71	575.44	572.5 [7] 563.9 [8]	572.79(15)[2]
$^{185}\text{Re}^{74+}$	455.96	458.36	451.0 [7] 448.6 [8]	456.05(30)[2]
$^{187}\text{Re}^{74+}$	451.69	454.06	-	451.69(30)[2]
$^{207}\text{Pb}^{81+}$	1019.1	1024.76	1020.5 [7] 1017.0 [8]	1019.7(2) [1]
$^{209}\text{Bi}^{82+}$	243.91	245.26	243.0 [7] 241.2 [8]	243.87(2) [1]
$^{203}\text{Tl}^{80+}$	385.89	388.01	383.98[6] 384.0 [7] 382.2 [8]	-
$^{205}\text{Tl}^{80+}$	382.79	384.89	380.22[6] 380.2 [7] 378.6 [8]	-
$^{207}\text{Tl}^{80+}$	377.68	379.74	-	-

References

- [1] I. Klaft *et al.*, Phys. Rev. Lett. **73**, 2425 (1993); P. Seelig *et al.*, Phys. Rev. Lett. **81**, 4824 (1998).
- [2] J. R. Crespo Lopez-Urrutia *et al.*, Phys. Rev. Lett. **77**, 826 (1996); Phys. Rev. A **57**, 879 (1998).
- [3] P. Beiersdorfer, private communication (2000).
- [4] M. Tomaselli, Ann. Phys. **205**, 362 (1991).
- [5] M. Tomaselli *et al.*, Phys. Rev. C **51** 2989 (1995); Phys. Rev. C **58**, 1524 (1998).
- [6] M.G.H. Gustavsson *et al.*, Hyperfine Interactions **127**, 437 (2000).
- [7] V.M. Shabaev *et al.*, Phys. Rev. A **56**, 252 (1997).
- [8] V.M. Shabaev, J. Phys. B **27**, 5825 (1994).
- [9] M. LeBellac, Nucl. Phys. **40**, 645 (1963).
- [10] S.M. Schneider *et al.*, Phys. Rev. A **50**, 118 (1994); H. Person *et al.*, Phys. Rev. Lett. **76**, 1433 (1996).
- [11] P. Sunergren *et al.* Phys. Rev. A **58**, 1055 (1998).

Asymptotic energy dependence of projectile inner-shell excitation cross sections in relativistic ion-atom collisions

Dorin Cezar Ionescu^{1,3} and Thomas Stöhlker^{1,2}

¹ Atomic Physics Division, Gesellschaft für Schwerionenforschung, D-64291 Darmstadt

² Institut für Kernphysik, J.W. Goethe Universität Frankfurt, D-60486 Frankfurt am Main

³ Institut für Theoretische Physik, Technische Universität Dresden, D-01062 Dresden

In recent years atomic collisions with ions moving with velocities close to the velocity of light have become experimentally feasible. While in the first place we are interested in a basic understanding of atomic phenomena for their own sake, a precise knowledge of the cross sections for collision processes is needed for certain aspects of the design and operation of accelerators. As an example, Coulomb excitation of electrons which is essential for stopping power investigations, is also an important production process for characteristic projectile photons in ion-atom encounters.

In particular, Coulomb excitation of heavy projectile ions enable the investigation of the influence of relativistic bound state wave functions on the dynamics in relativistic ion-atom collisions. In addition, such studies provide detailed information on the effects associated with the Liénard-Wiechert interaction between the active electron and the target nucleus [1]. Thus, with increasing energy spin-flip mediated transitions were shown to become quite important above roughly 100 MeV/u such that contributions associated with the velocity dependent (magnetic) part of the time dependent interaction are quite relevant. In contrast to ionization where measured total cross sections are available for highly-charged ions up to uranium for more than one decade, it was only recently that detailed experimental data on the K -shell excitation of high- Z projectile ions were reported [1, 2].

In the present investigation we elucidate further details of the mechanisms associated with the Coulomb excitation of high- Z_P projectiles by considering the asymptotic energy dependence of the relevant cross sections. Specifically, we extend our previous results into the extreme relativistic energy domain with energies of hundreds of GeV/u. The numerical calculations are complemented by an analytic representation of the asymptotic energy dependence of cross sections which brings additional insight. The projectile ion is chosen as the origin of the coordinate system such that the target provides the time dependent perturbation mediating the transition.

In Figure 1 we show the energy dependence of reduced cross sections σ/Z_T^2 for exciting a K -shell electron in hydrogen-like gold colliding with an atomic target with charge number Z_T . The cross sections are divided by Z_T^2 which is the scaling behavior in lowest-order perturbation theory. We consider the ($Ly-\alpha_1$) transition of a $1s_{1/2}$ spin-up electron ($\mu_i = 1/2$) to the $2p_{3/2}$ ($\mu_f = \pm 1/2, \pm 3/2$) states of the projectile ion (Au^{78+}). The upper curve (Σ) is associated with the total $Ly-\alpha_1$ cross section, the dashed (short-dashed) curve corresponds to the transition with $\Delta\mu = \mu_f - \mu_i = +1$ (spin-flip), and the dotted (dott-dashed) curve is related to $\Delta\mu = +2$ (0).

The present numerical results demonstrate that cross

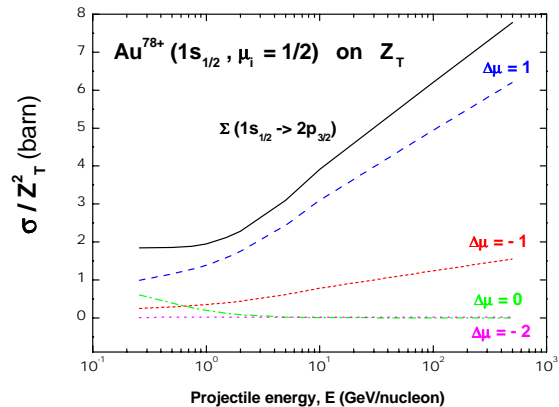


Figure 1: Reduced cross sections σ/Z_T^2 for projectile excitation as functions of the laboratory energy.

sections associated with transitions where the magnetic quantum number changes by one unit ($\Delta\mu = \pm 1$) increase with increasing energy roughly as $\ln E$ in the region above 1 GeV/u. In contrast, the cross sections associated with the other types of transitions ($\Delta\mu = 0, 2$) decrease with increasing collision energy, and approach zero in the asymptotic energy region. Note that the inclusion of screening would lead to different energy dependence [3]. As a result, the cross section for the unscreened $Ly-\alpha_1$ transition is provided solely by the $\Delta\mu = \pm 1$ transitions for collision energies in the GeV/u region and higher.

An interesting parallel can be made with a computationally simple treatment of the excitation process in the Fermi-Weizsäcker-Williams (FWW) approximation. There the actual electromagnetic field created by the moving ions is approximated by the field associated with a swarm of real photons. In addition, a free parameter which is related to the maximum photon energy is to be fixed (in some sense arbitrary), such that the domain of applicability of the method is often not clear. From Figure 1 one can see that above roughly 3 GeV/u only transitions with $\Delta\mu = \pm 1$ provide a nonzero contribution to the cross section. Thus, the present investigation provides a quantitative measure of the range that can be treated safely in a computationally simple FWW scheme.

References

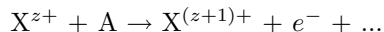
- [1] Th. Stöhlker et al., Phys. Rev. A **57**, 845 (1998); Phys. Lett. A **238**, 43 (1998).
- [2] T. Ludziejewski et al., Phys. Rev. A **61**, 052706-1 (2000).
- [3] A.H. Sorensen, Phys. Rev. A **58**, 2895 (1999).

Stripping of Fast Heavy Low-Charged Ions in Gases

V. Shevelko (GSI and P.N. Lebedev Institute, Moscow),
T. Stöhlker (GSI)

Electron loss and capture processes arising in collisions of heavy low-charged ions with atoms and ions are the main charge-changing reactions in heavy-ion driven inertial fusion (HIDIF) [1]. However, at present time, virtually no experimental and theoretical data are available for removal processes involving fast heavy low-charged ions.

In this work, the projectile-ionization (stripping) cross sections and beam lifetimes in reactions



have been calculated for ions $X = \text{Xe}, \text{Pb}, \text{Bi}, \text{U}$ ($z < 10$) colliding with neutral atoms $A = \text{H}, \text{He}, \text{Be}, \text{C}, \text{F}, \text{N}, \text{Ar}, \text{Xe}$ in the $E = 1 - 100 \text{ MeV/u}$ energy range. Calculations have been performed for *single*-electron stripping in the first-order perturbation theory using the LOSS computer code. The atomic structure of the target was taken into account in the form of its atomic form-factor $F(q)$ depending on the momentum transfer q .

For the case of ionization of Pb-like ions ($\text{Xe}^{0+}, \text{Bi}^{1+}, \dots, \text{U}^{10+}$) and the energy range considered, a scaling law for stripping cross sections was obtained in the form:

$$\tilde{\sigma} = \sigma \cdot (I_P/Z_T)^{1.4}, \quad \tilde{E} = E/I_P, \quad (1)$$

where I_P is the *first* ionization potential of the projectile in eV, E is the beam energy in eV/u, and Z_T denotes the target nuclear charge. The scaled cross sections for Pb-like ions are displayed in Fig. 1 in comparison with available experimental data and other calculations (see [2] in detail); $1 \text{ Ry} = 13.606 \text{ eV}$.

Ion-beam lifetimes τ have been calculated with account for electron capture processes using the CAPTURE computer code. The values of τ are shown in Fig. 2. A small minimum for U^{28+} ions around 2 MeV/u is related to the influence of electron capture which for these ions prevails at energies $E < 10 \text{ MeV/u}$.

A comparison of the present calculations with experimental data [3]–[5], classical-trajectory Monte-Carlo (CTMC) calculations [6] and $Z_T^2 + Z_T$ scaling [7] shows the following peculiarities for the stripping processes of heavy low-charged ions in neutral targets:

1) the contribution from ionization of the projectile inner-shell electrons is very significant, and, in calculations, one has to account for 6–8 inner subshells,

2) at high energies, the stripping cross sections fall off approximately as $\sigma \sim E^{-1}$,

3) multiple-ionization processes seem to play a very important role and, according to [6], their contribution can reach up to 50 % to the total stripping cross section.

References

- [1] I. Hofmann, G. Plass (eds.): *The HIDIF-Study*, Report GSI-98-06, Darmstadt (1998)
- [2] I.Yu. Tolstikhina, V.P. Shevelko, Th. Stöhlker: Preprint GSI-2000-54, Darmstadt (2000)

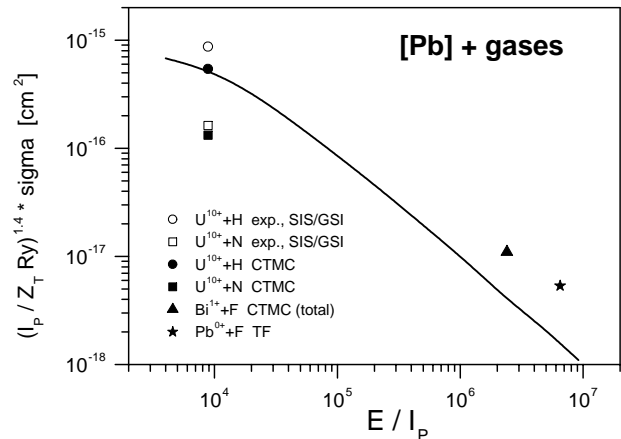


Figure 1: Scaled ionization cross sections of Pb-like ions colliding with neutral atoms, eq. (1). Solid curve – present result, symbols – experimental and theoretical data (see [2] in detail).

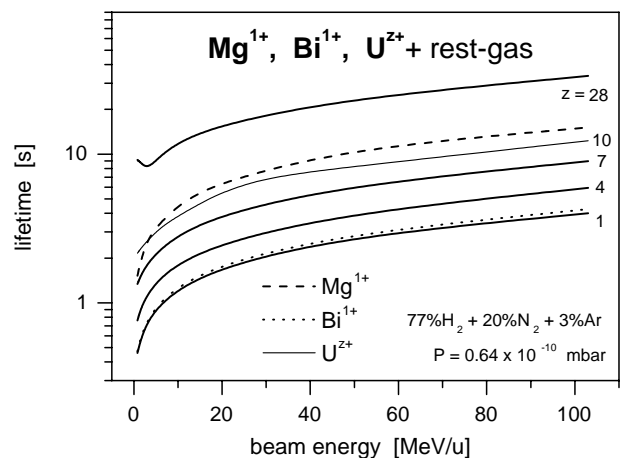


Figure 2: Beam lifetimes of ions colliding with a residual gas mixture and a gas pressure indicated in the figure – present result.

- [3] W. Erb: Report GSI-P-78, Darmstadt (1978)
- [4] B. Franzke: IEEE, NS-28, 2116 (1981)
- [5] K. Blasche et al.: GSI Scientific Report 1996, Darmstadt (1997), p. 159
- [6] R. Olson: Proc. HIF-2000, San Diego (Febr. 2000) (in press)
- [7] V.P. Shevelko et al.: Hyp. Int. **114**, 289 (1998); V.P. Shevelko et al.: NIM A **415**, 609 (1998)

